AD-A181 421 THE USE OF NOVEL PROCESSING PROCEDURES FOR IMPROVING 1/1
OVERALL FATIGUE RESI (U) VIRGINIA UNIV CHARLOTTESVILLE
DEPT OF MATERIALS SCIENCE E A STARKE ET AL MAY 87
UNCLASSIFIED UVA/525644/MS87/102 AFOSR-TR-87-0730 F/G 11/6 2 NL

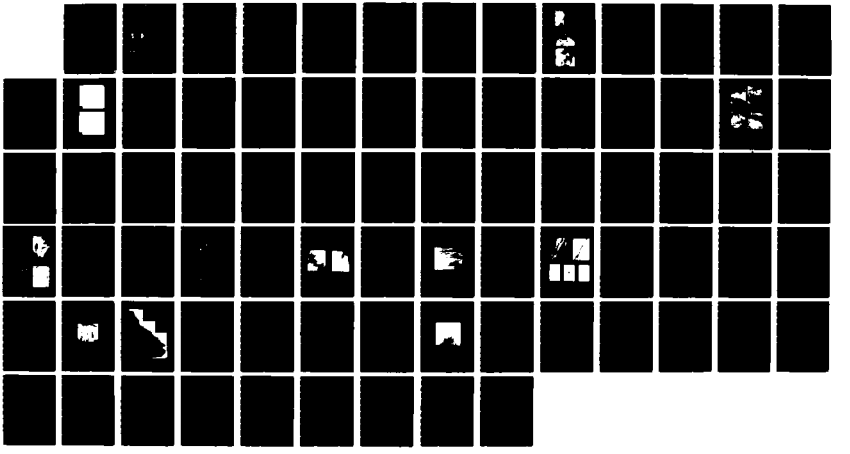

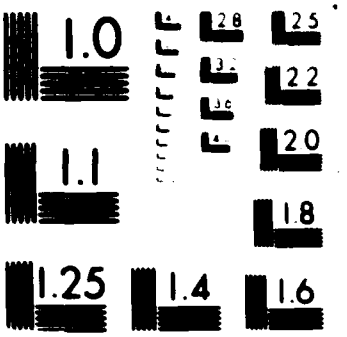
1.0
1.1
1.25
1.4
1.6
1.8
2.0
2.2
2.5

AFOSR-TR- 87-0730

A Final Report
Contract No. AFOSR-83-0061-
January 1, 1984 - December 31, 1986

THE USE OF NOVEL PROCESSING PROCEDURES FOR IMPROVING OVERALL FATIGUE RESISTANCE OF HIGH STRENGTH ALUMINUM ALLOYS

Submitted to:

Air Force Office of Scientific Research, NE
Building 410
Bolling Air Force Base
Washington, D.C. 20332

Attention: Alan H. Rosenstein

Submitted by:

Edgar A. Starke, Jr.
Earnest Oglesby Professor and Dean

J. A. Wert
Associate Professor

Report No. UVA/525644/MS87/102
May 1987

SCHOOL OF ENGINEERING AND APPLIED SCIENCE

DEPARTMENT OF MATERIALS SCIENCE

UNIVERSITY OF VIRGINIA
CHARLOTTESVILLE, VIRGINIA 22901

UNCLASSIFIED
SECURITY CLASSIFICATION OF THIS PAGE

AD-A181 421

REPORT DOCUMENTATION PAGE

1a. REPORT SECURITY CLASSIFICATION Unclassified	1b. RESTRICTIVE MARKINGS None
2a. SECURITY CLASSIFICATION AUTHORITY	3. DISTRIBUTION/AVAILABILITY OF REPORT Approved for public release; distribution unlimited
2b. DECLASSIFICATION/DOWNGRADING SCHEDULE	
4. PERFORMING ORGANIZATION REPORT NUMBER(S) UVA/525644/MS87/102	5. MONITORING ORGANIZATION REPORT NUMBER(S) AFOSR-TR- 87-0730
6a. NAME OF PERFORMING ORGANIZATION University of Virginia Dept. of Materials Science	6b. OFFICE SYMBOL (If applicable)
7a. NAME OF MONITORING ORGANIZATION Air Force Office of Scientific Research/PKD	
6c. ADDRESS (City, State, and ZIP Code) Department of Materials Science Thornton Hall Charlottesville, VA 22901	7b. ADDRESS (City, State, and ZIP Code) Building 410 Bolling Air Force Base Washington, DC 20332-6448
8a. NAME OF FUNDING/SPONSORING ORGANIZATION AFOSR/NE	8b. OFFICE SYMBOL (If applicable) NE
9. PROCUREMENT INSTRUMENT IDENTIFICATION NUMBER AFOSR-83-0061-B	
8c. ADDRESS (City, State, and ZIP Code) Building 410 Bolling Air Force Base Washington, DC 20332-6448	10. SOURCE OF FUNDING NUMBERS PROGRAM ELEMENT NO. 61102F; PROJECT NO. 2306; TASK NO. A1; WORK UNIT ACCESSION NO.

11. TITLE (Include Security Classification) The Use of Novel Processing Procedures For Improving Overall Fatigue Resistance of High Strength Aluminum Alloys

12. PERSONAL AUTHOR(S)
E. A. Starke, Jr.; J. A. Wert

13a. TYPE OF REPORT	13b. TIME COVERED	14. DATE OF REPORT (Year, Month, Day)	15. PAGE COUNT
Final	FROM 1/1/84 TO 12/31/86	1987 May	70

16. SUPPLEMENTARY NOTATION

17. COSATI CODES			18. SUBJECT TERMS (Continue on reverse if necessary and identify by block number)
FIELD	GROUP	SUB-GROUP	
			Zirconium, sq. mm

19. ABSTRACT (Continue on reverse if necessary and identify by block number)

In Part 1 of this investigation, ductile fracture of 2134 aluminium alloys stabilized by Zr has been studied as a function of Mn rich particle content in the under and overaged conditions. As expected in the highest Mn containing alloy voids/mm², void growth rate, and void volume fraction were the highest whereas in alloys with 0% and 0.31% Mn these parameters were somewhat similar and lower. This resulted in the least ductility and fracture toughness in the 1.02% Mn alloy. However the ductility level -- percent reduction in area and the true fracture strain -- in the overaged condition is found to be higher than in the underaged for any given manganese level in spite of higher void nucleation rate and void growth rate. This suggests that the final void coalescence mechanism in the ductile fracture plays a more dominant role than nucleation and growth in reducing the ductility in the underaged

20. DISTRIBUTION/AVAILABILITY OF ABSTRACT	21. ABSTRACT SECURITY CLASSIFICATION
☒ UNCLASSIFIED/UNLIMITED ☐ SAME AS RPT ☐ DTIC USERS	Unclassified
22a. NAME OF RESPONSIBLE INDIVIDUAL Alan H. Rosenstein	22b. TELEPHONE (Include Area Code) 202-767-4984
	22c. OFFICE SYMBOL NE

DD FORM 1473, 84 MAR — 83 APR edition may be used until exhausted. All other editions are obsolete

SECURITY CLASSIFICATION OF THIS PAGE
UNCLASSIFIED

condition. Generally the final stage occurs by localization of slip in between two large size voids. It appears that the underaged alloys which already deform by planar slip mode enhance the slip localization process resulting in earlier coalescence of voids along these slip bands formed in between large sized voids.

cont'd

Part 2 of this investigation has examined intergranular fracture during heat treatment and deformation of an Al-Li-Cu alloy and an Al-Li-Cu-Mg alloy. When the Al-Li-Cu-Mg alloy used in this study is solution treated by rapid heating to 550°C, nonequilibrium eutectic melting of a soluble phase occurs. The liquid spreads along grain boundaries as a thin film, which solidifies by diffusion of solute into the adjoining grains. Upon quenching, intergranular cracks are found at grain boundaries where a liquid film had formed during solution treatment. At solution treatment temperatures of 530°C and below, nonequilibrium eutectic melting did not occur and no intergranular cracks were found in as-quenched specimens. The eutectic melting is associated with a soluble precipitate phase. No evidence of nonequilibrium eutectic melting was found in the companion Al-Li-Cu alloy.

For the Al-Li-Cu-Mg alloy, intergranular fracture occurred during tensile testing of as-quenched and quenched-and-aged specimens, irrespective of whether nonequilibrium eutectic melting had taken place during solution treatment. For the Al- Li-Cu alloy, intergranular fracture occurred during tensile testing of quenched-and-aged specimens, but not of as-quenched specimens. The cause of intergranular fracture during deformation of these alloys is unlikely to be segregation of Na and K impurities to grain boundaries. Several additional explanations for intergranular fracture have previously been proposed, but the available evidence in the present case does not strongly support or exclude any of the remaining explanations.

A Final Report
Contract No. AFOSR-83-0061-C
January 1, 1984 - December 31, 1986

THE USE OF NOVEL PROCESSING PROCEDURES FOR IMPROVING OVERALL FATIGUE RESISTANCE OF HIGH STRENGTH ALUMINUM ALLOYS

Submitted to:

Air Force Office of Scientific Research/NE
Building 410
Bolling Air Force Base
Washington, D.C. 20332

Attention: Alan H. Rosenstein

Submitted by:

Edgar A. Starke, Jr.
Earnest Oglesby Professor and Dean

J. A. Wert
Associate Professor

Department of Materials Science
SCHOOL OF ENGINEERING AND APPLIED SCIENCE
UNIVERSITY OF VIRGINIA
CHARLOTTESVILLE, VIRGINIA

Report No. UVA/525644/MS87/102
May 1987

Copy No. 9

TABLE OF CONTENTS

Part 1. Ductile Fracture of 2134 Aluminum

J. A. Walsh, K. V. Jata and E. A. Starke, Jr.

Abstract of Part 1

Ductile fracture of 2134 aluminium alloys stabilized by Zr has been studied as a function of Mn rich particle content in the under and overaged conditions. As expected in the highest Mn containing alloy voids/mm^2, void growth rate, and void volume fraction were the highest whereas in alloys with 0% and 0.31% Mn these parameters were somewhat similar and lower. This resulted in the least ductility and fracture toughness in the 1.02% Mn alloy. However the ductility level -- percent reduction in area and the true fracture strain -- in the overaged condition is found to be higher than in the underaged for any given manganese level in spite of higher void nucleation rate and void growth rate. This suggests that the final void coalescence mechanism in the ductile fracture plays a more dominant role than nucleation and growth in reducing the ductility in the underaged condition. Generally the final stage occurs by localization of slip in between two large size voids. It appears that the underaged alloys which already deform by planar slip mode enhance the slip localization process resulting in earlier coalescence of voids along these slip bands formed in between large sized voids.

1.1 Effects of Mn Rich Particles on Ductile Fracture of 2134 Type Alloys

1.1.1 Microstructure of the Alloys

The chemical composition of the alloys that were studied is given in Table 1. The large second phase particles in alloy #1 that do not contain any Mn are Al_2CuMg, whereas for the alloys which contain Mn, the large particles are both Al_2CuMg and $Al_{20}Cu_2Mn_3$. Table 2 shows the distribution and spacing parameters of these large particles,

which were determined at a magnification of 300X on the SEM. The next size particles which were observed on the TEM are shown in Figure 1. The grain size of all these alloys were determined and was observed to be similar.

Table 1. Chemical Composition in weight percent

Alloy	Cu	Mg	Mn	Fe	Si	Zr
# 1	3.96	1.48	----	.06	.04	.14
# 2	3.96	1.46	0.31	.06	.04	.12
# 4	4.51	1.47	1.02	.06	.04	.12

Table 2. Particle Distribution and Spacing Parameters Determined at 300 X

Alloy	V_v	$N_A(mm^{-2})$	$N_L(mm^{-1})$	l(mm)	s(mm)
#1	0.0175	589	5.42	0.18	0.18
#2	0.0196	686	5.50	0.18	0.18
#4	0.0407	1129	10.56	0.091	0.095

1.1.2 Mechanical Properties

Standard tensile tests on 25 mm gage length cylindrical samples in the longitudinal direction were performed at a strain rate of 3×10^{-3} sec. The yield strength of all the alloys was kept constant by suitably changing the aging time at 190°C. The mechanical properties obtained from the tensile data are shown in Table 3. The strain hardening exponent in the underaged condition was found to be higher than in the overaged condition. The true fracture strain and percent reduction in area are shown in Figure 2 as a function of weight % Mn. In both the under and overaged alloys 0.31% Mn provides an increase in

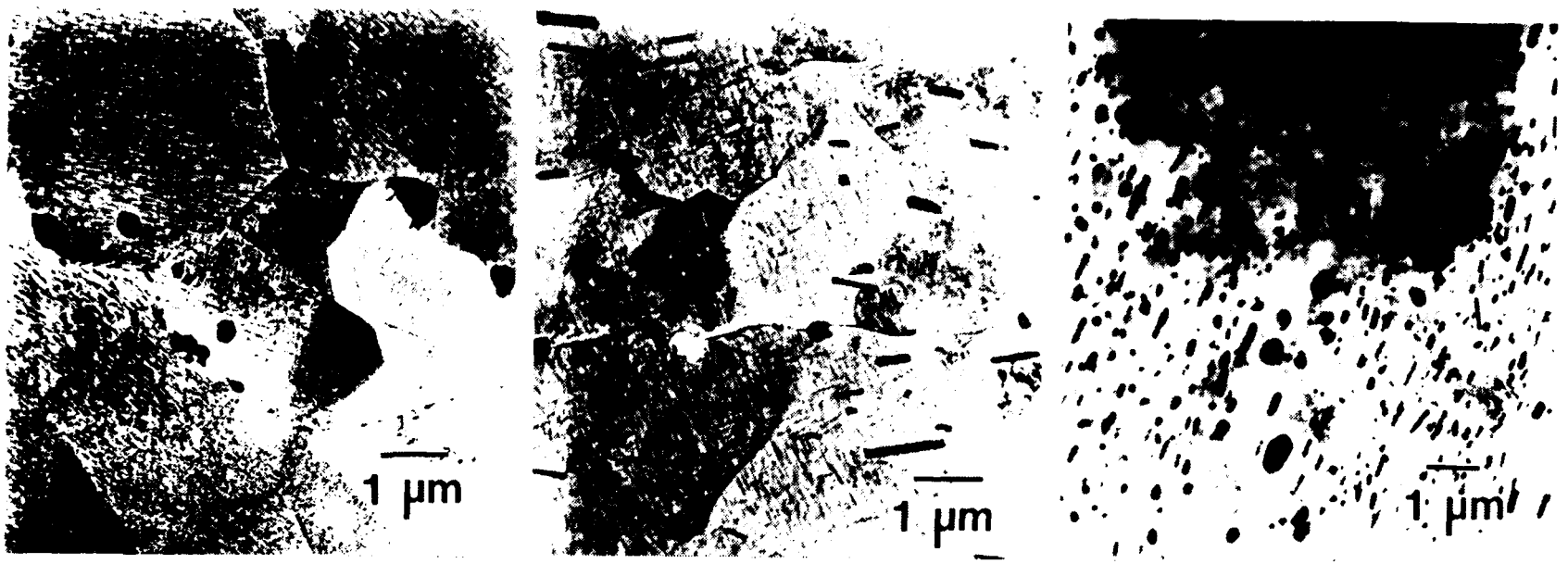

0% Mn Alloy

0.31% Mn Alloy

1.02% Mn Alloy

Figure 1: Mn rich particle distribution.

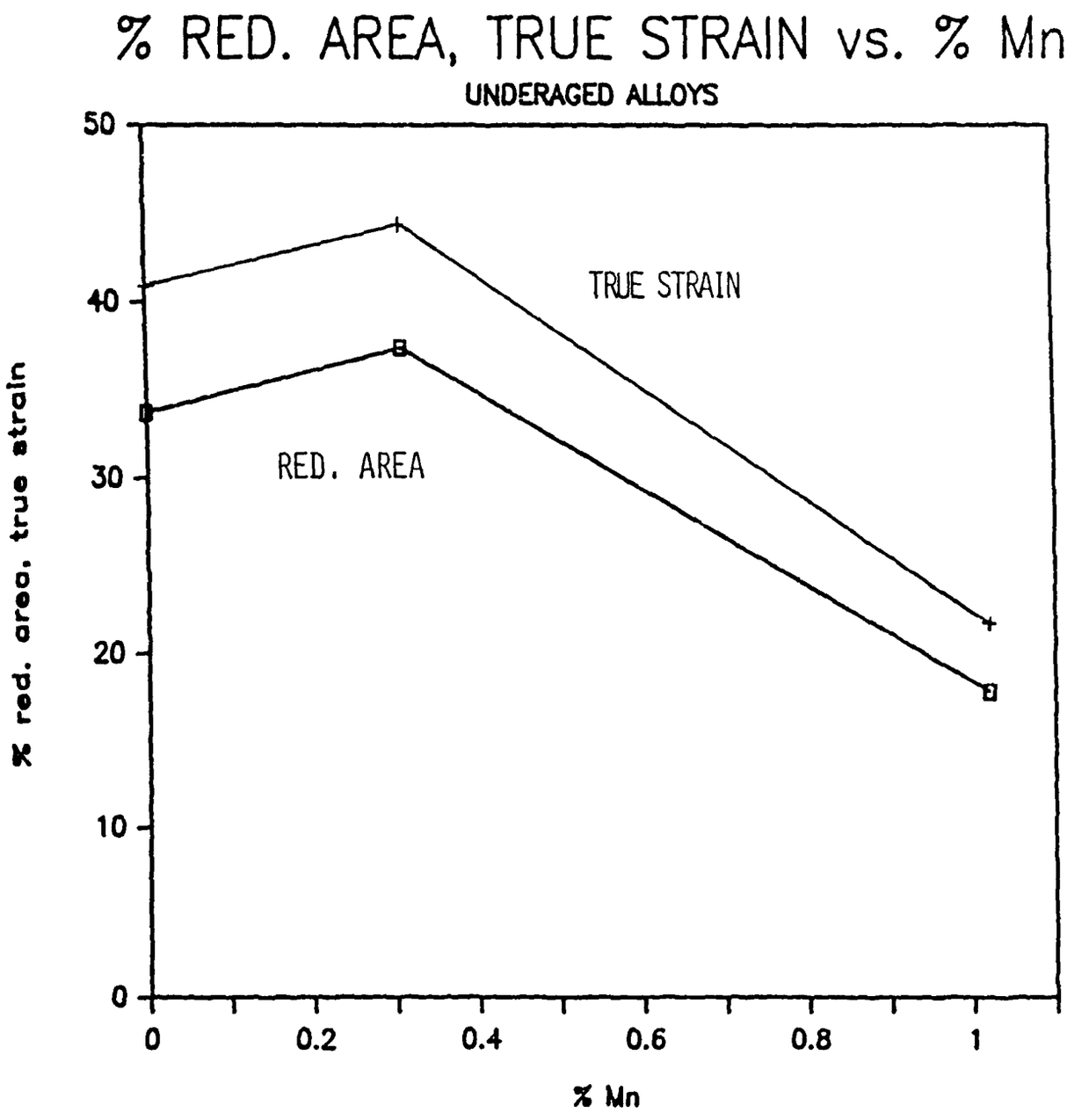
% RED. AREA, TRUE STRAIN vs. % Mn
UNDERAGED ALLOYS
TRUE STRAIN
RED. AREA
% red. area, true strain
% Mn
50
40
30
20
10
0
0
0.2
0.4
0.6
0.8
1

Figure 2a

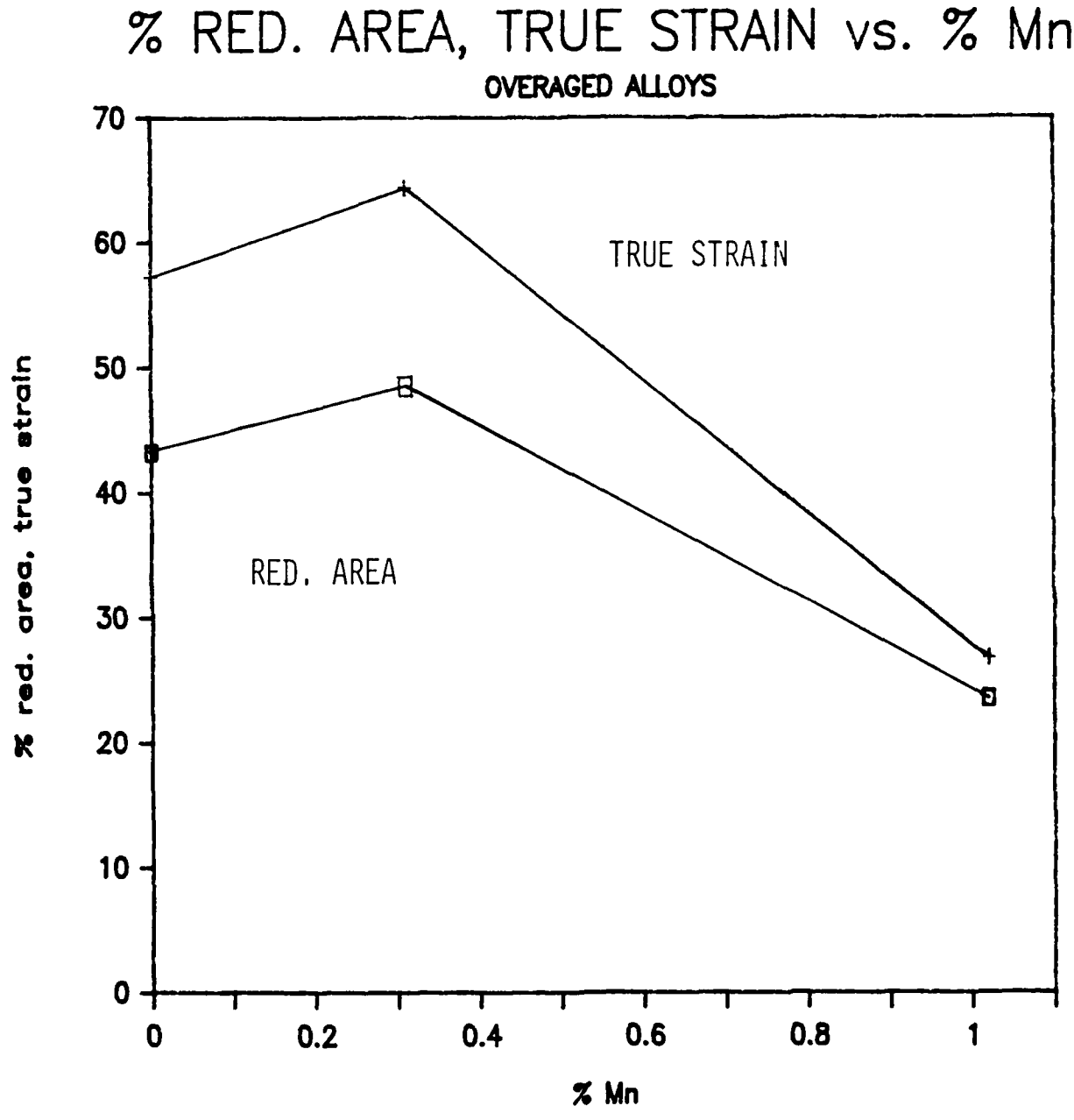
% RED. AREA, TRUE STRAIN vs. % Mn
OVERAGED ALLOYS
TRUE STRAIN
RED. AREA
% red. area, true strain
% Mn
70
60
50
40
30
20
10
0
0
0.2
0.4
0.6
0.8
1

Figure 2b

ductility. With 1.02% Mn, the ductility drops drastically. All the overaged alloys demonstrate higher fracture ductility than the underaged alloys.

Table 3. Room Temperature Mechanical Properties

Alloy	σ_{ys}(MPa)	σ_{uts}(MPa)	n	%el.	ε_{ft}	% RA	K1c(MPa $m^{\frac{1}{2}}$)
#1 UA	376	431	.052	11.2	.409	33.7	52
OA	447	481	.036	13.5	.573	43.2	39
#2 UA	403	443	.065	15.7	.444	37.4	53
OA	448	478	.037	10.3	.644	48.8	45
#4 UA	425	491	.057	13.4	.217	17.8	32
OA	451	493	.041	9.5	.268	23.5	27

1.1.3 Void Volume Fraction

The combined effects of void nucleation and growth were studied by measuring the void volume percent in the deformed gage section for increasing strain levels, Figure 3. We obtained density measurements by using a picnometer from the deformed gage section and the undeformed grip section yielding the void volume percent only from deformation thereby eliminating local variations in the alloy due to aging or processing. Alloy #4 (1.02% Mn) shows a much higher rate of increase of void volume percent -- 3% per unit strain -- than does alloys #1 and #2 -- 0.7% per unit strain. The differences in the under and over aged alloys at least at the strain levels studied so far were negligible in #1 and #2 alloys. However in #4 alloy the overaged condition shows slightly lower values although one would expect the opposite behaviour due to the presence of equilibrium precipitates in the overaged condition. These observations will be double checked by using a automated picnometer that is currently available. The next step was to seperate the nucleation and growth effects for the different alloys in the two aging conditions.

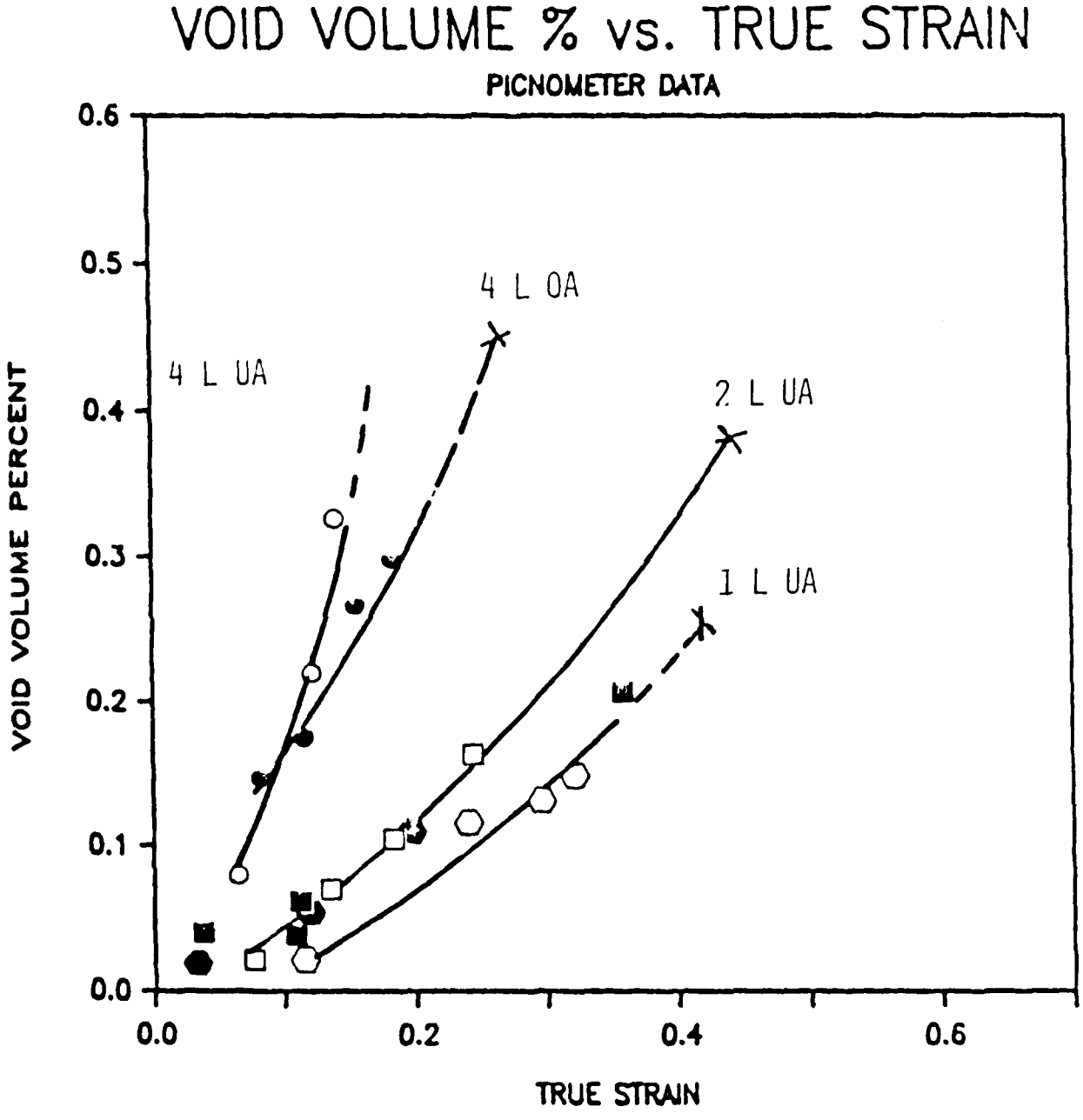
VOID VOLUME % vs. TRUE STRAIN
PICNOMETER DATA
VOID VOLUME PERCENT
TRUE STRAIN
0.0
0.1
0.2
0.3
0.4
0.5
0.6
0.0
0.2
0.4
0.6
4 L OA
4 L UA
2 L UA
1 L UA

Figure 3

1.1.4 Areal Void Density

Void nucleation and growth effects were studied on longitudinally sectioned specimens strained to various strains. Voids associated with large second phase particles are shown in Figure 4. In these micrographs one can see that particle fracture dominates void nucleation with some particle decohesion also occuring at smaller spherical Mg containing particles. The large irregular shaped particles often displayed multiple cracking and were generally found to be $Al_{20}Cu_2Mn_3$ particles. The areal void density as a function of strain is shown in Figure 5. This curve suggests the increasing nucleation of voids as a function of strain. The differences in alloy #1 and #2 in both the under and overaged conditions is negligible and the curves for the two alloys overlap. However more data needs to be generated to confirm this statement. For both the under and overaged alloys #4 is nucleating more voids for any given strain level than #1 and #2 and at a much faster rate as indicated by the slopes. More voids nucleate in #4 than #1 or #2 because there are more nucleation sites in #4. However there are only twice as many potential nucleation sites as indicated by the volume fraction of large second phase particle sites and the number of voids/mm^2 for #4 for any strain is more than double that of #1 or #2. For example in the overaged condition at 0.2 strain, alloy #4 has 1150 voids/mm^2 whereas alloy #2 exhibits 100 voids/mm^2. There are two reasons for this factor of eleven difference: (1) each particle has multiple nucleation sites and (2) because of the closer particle spacing in alloy #4 the stress and strain fields may interact giving rise to a higher local stress or strain.

In comparing alloy #4 in the under and overaged condition the overaged alloy has a more dense population of voids than the underaged

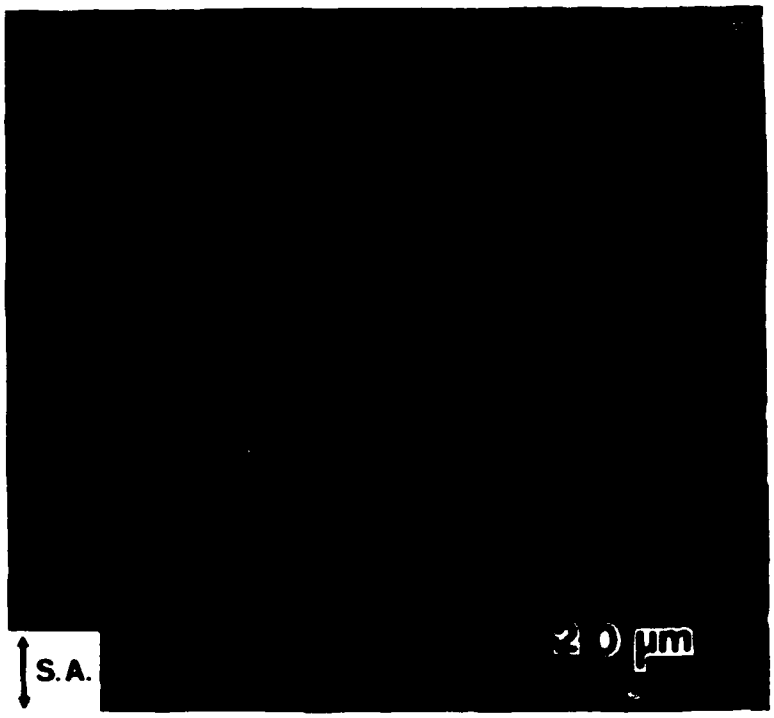

1.02% Mn

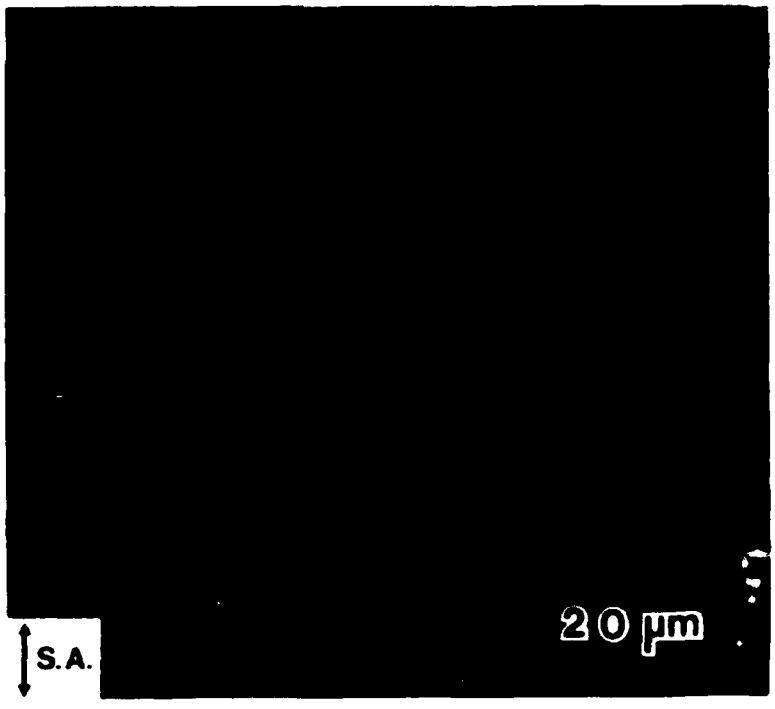

0.0% Mn

Figure 4: Voids at particles.

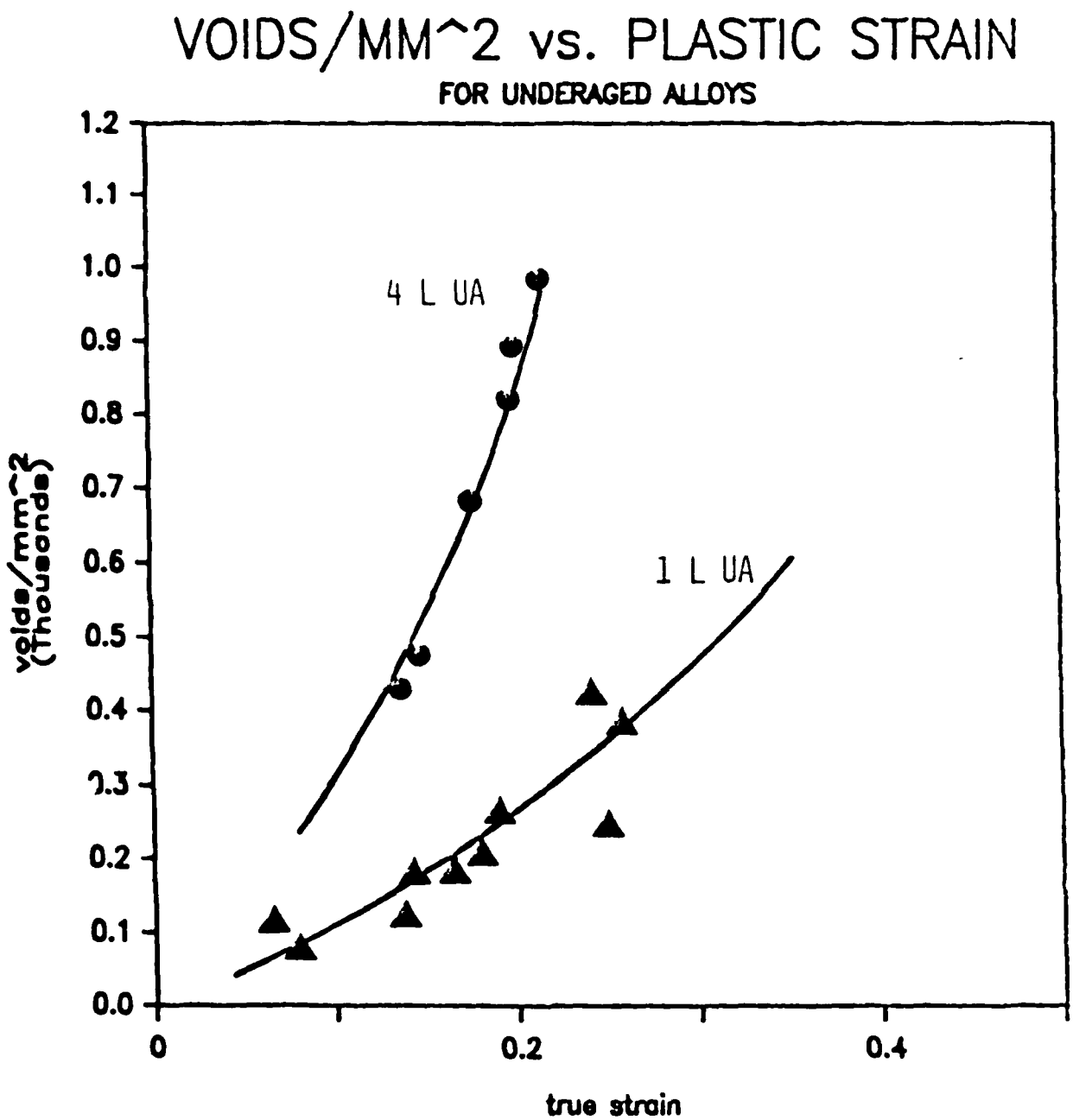
VOIDS/MM^2 vs. PLASTIC STRAIN
FOR UNDERAGED ALLOYS
4 L UA
1 L UA
voids/mm^2 (thousands)
true strain
1.2
1.1
1.0
0.9
0.8
0.7
0.6
0.5
0.4
0.3
0.2
0.1
0.0
0
0.2
0.4

Figure 5a

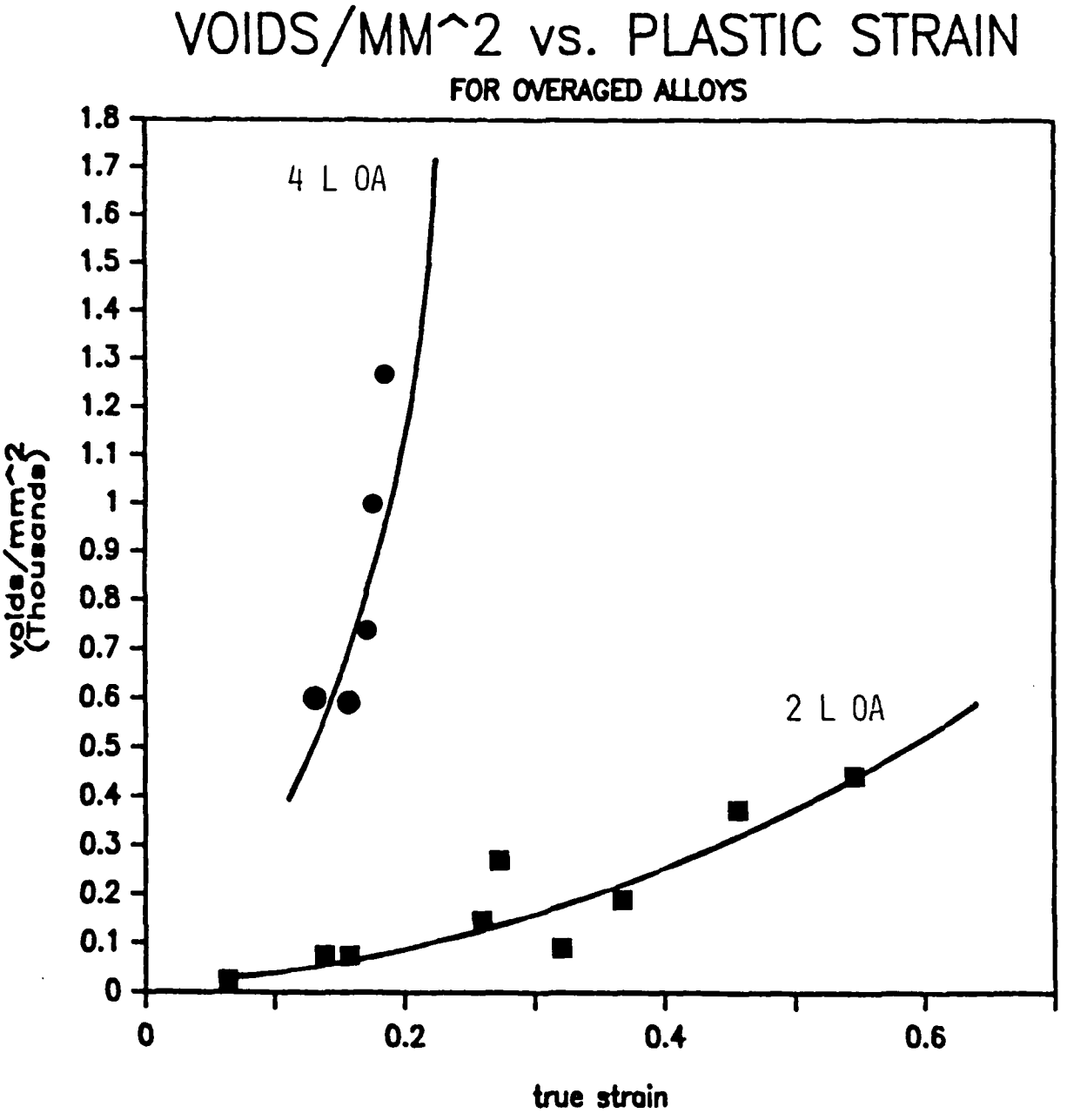
VOIDS/MM^2 vs. PLASTIC STRAIN
FOR OVERAGED ALLOYS
4 L OA
2 L OA
voids/mm^2 (Thousands)
true strain
1.8
1.7
1.6
1.5
1.4
1.3
1.2
1.1
1
0.9
0.8
0.7
0.6
0.5
0.4
0.3
0.2
0.1
0
0
0.2
0.4
0.6

Figure 5b

alloy for any given strain. The deformed tensile specimens also showed a much earlier neck formation in the overaged case than in the underaged; 0.08 strain as opposed to 0.15 strain. This early necking in the overaged samples could be due to homogeneous deformation as compared to heterogeneous deformation in the underaged alloys. The necking is accompanied by an increasing amount of triaxial stress providing higher local stress in the overaged alloys and facilitating void nucleation.

1.1.5 Void Growth

The maximum void size along the stress axis as a function of strain is shown in Figure 6. The slopes of these curves at present have been assumed constant and therefore a linear plot is shown. Further investigations at higher strain levels where deeper necks and higher triaxiality levels are achieved will determine if the maximum void size should rise exponentially with strain yielding a exponentially increasing void growth rate. The constant void growth rates and ductilities are shown in Table 5.

Table 4. Void Growth Rates

Alloy	Void Growth Rate (μm/unit strain)	Ductility (% RA)
2 UA	16	33.7
4 UA	34	17.8
2 OA	17	43.2
4 OA	75	23.5

In each aging condition as the Mn level increases ductility decreases and the void growth rate increases. This could be explained

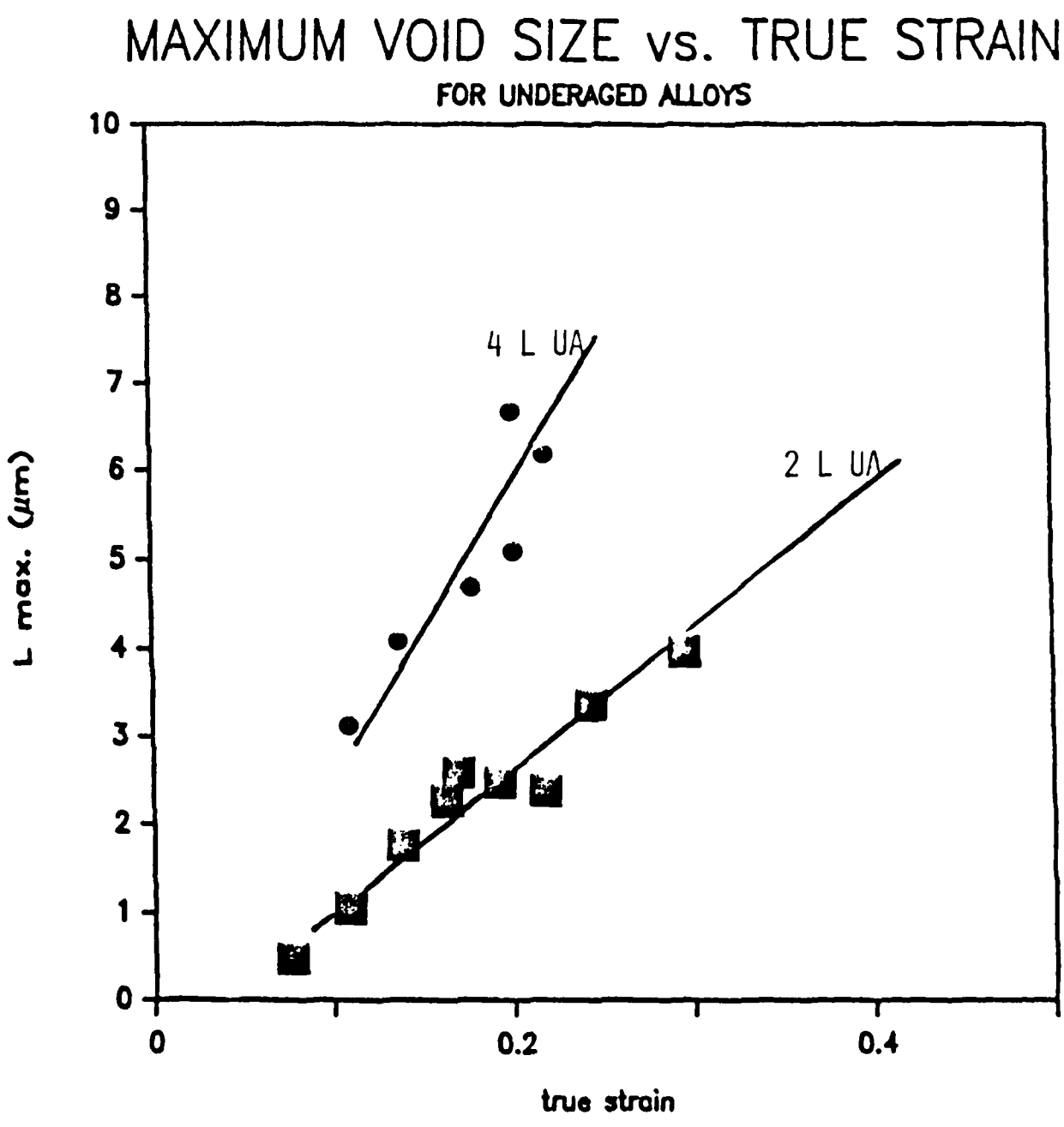
MAXIMUM VOID SIZE vs. TRUE STRAIN
FOR UNDERAGED ALLOYS
L max. (μm)
true strain
4 L UA
2 L UA
0
1
2
3
4
5
6
7
8
9
10
0
0.2
0.4

Figure 6a

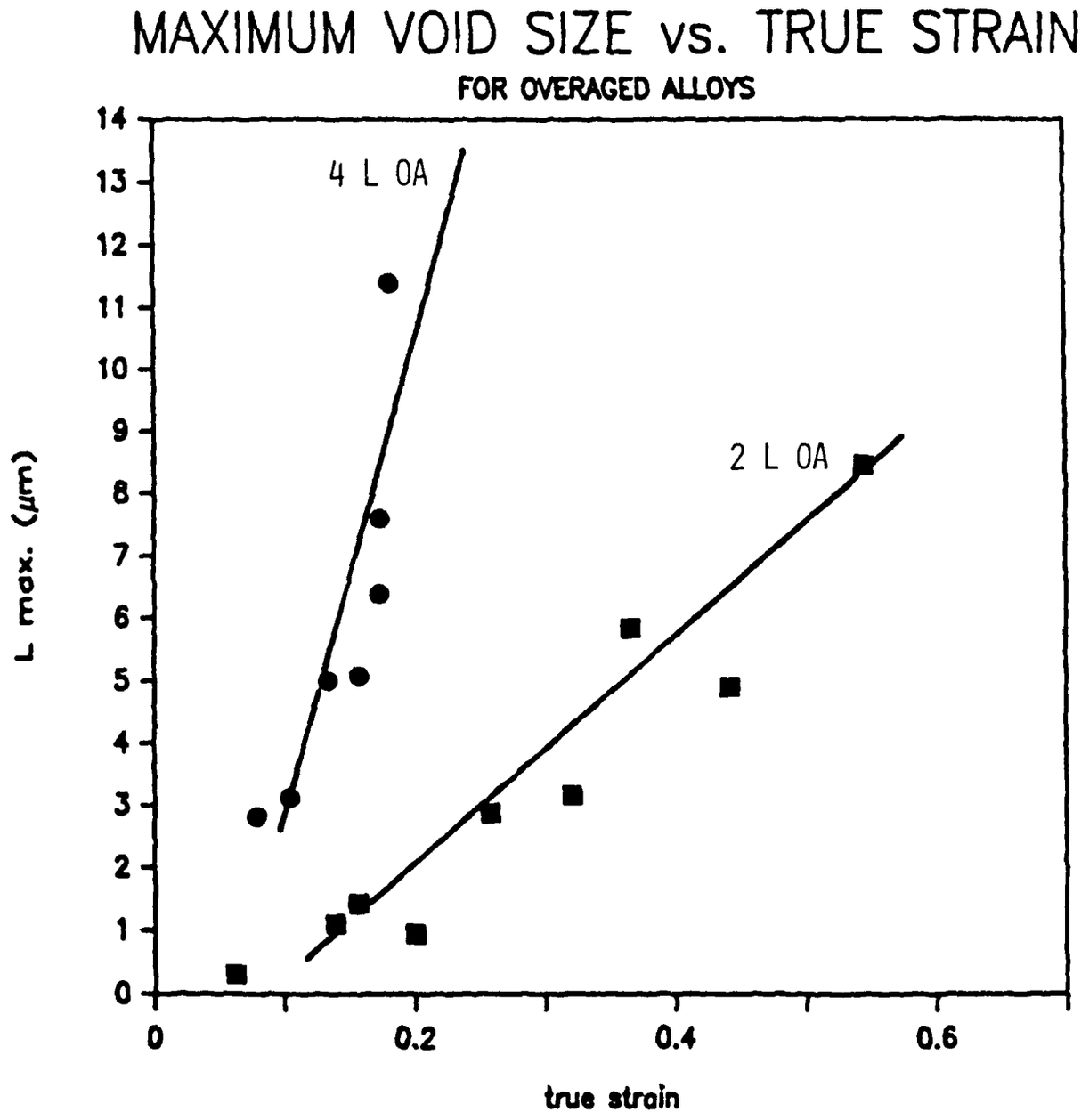
MAXIMUM VOID SIZE vs. TRUE STRAIN
FOR OVERAGED ALLOYS
4 L OA
2 L OA
L max. (μm)
true strain
0
1
2
3
4
5
6
7
8
9
10
11
12
13
14
0
0.2
0.4
0.6

Figure 6b

on the basis of closer spacing of the voids due to closely spaced particles. However the ductility in the overaged condition for any one alloy increases even though the void growth rate remains constant for #2 or increases for #4. This suggests that although localized planar slip in the underaged condition does not provide a greater damage accumulation overall, it does provide local critical damage.

1.1.6 Fracture Toughness

The fracture toughness values obtained from compact tension specimens are shown in Table 3. In the underaged alloys these values stay about the same in #1 and #2 alloys whereas in #4 there is a decrease. However, in the overaged alloys an increase in fracture toughness is observed at first, and then a decrease in the #4 alloy. Thus a dependence of K_{IC} on the large particle spacing, Tables 3 and 2 , is not clearly evident in #1 and #2 alloys. In the overaged alloys, the fracture toughness increases from 39 MPa $m^{\frac{1}{2}}$ to 45 MPa $m^{\frac{1}{2}}$ with no change in particle spacing (0.18 mm). This increase appears to contradict expected results. However, even though the spacing of the large particles remains the same, the distribution of small (~0.5 μm) dispersoids particles increases, thereby further homogenizing the slip and increasing the fracture toughness. These dispersoid distributions for the #1, #2, and #4 alloys can be seen in the TEM micrographs in Figure 1. The fracture toughness drops to 27 MPa $m^{\frac{1}{2}}$ in #4 with a corresponding drop in particle spacing. In this alloy, the beneficial effect of the dispersoids is lost because the Mn rich particles, Figure 1, become too abundant and too large and the void sheet formation occurs over much shorter distances. The dispersoids do not form voids until late in the deformation process. Prior to forming voids, they

homogenize deformation, and are therefore beneficial to the fracture toughness of the alloy. This is reflected in the fracture toughness values of #1 and #2 alloys. In the underaged alloys, the spacing of large second phase particles does not change in alloys #1 and #2 (0.18 mm), but neither does the fracture toughness (52 MPa $m^{\frac{1}{2}}$). The spacing decreases to 0.091 mm in alloy #4 with the expected drop in fracture toughness to 32 MPa $m^{\frac{1}{2}}$. The slip homogenizing effect of the dispersoids in the underaged condition is superceeded by the planar slip and thus they do not improve the K_{IC} as compared to #1.

1.1.7 Conclusions

Void intiation in all the alloys occurs at large undissolved Al_2CuMg particles, large Mn rich particles and constituent particles.

The rate of increase of void fraction in #4 alloy (3%/unit strain) is greater than #1 and #2 alloys (0.7%/unit strain) because the larger particles are more closely spaced enabling void link up . The areal void density in #4 alloy is also greater than in #1 and #2 because of a higher void nucleating particle density.

The addition of manganese improves ductility and fracture toughness because the Mn rich dispersoids enables homogeneous deformation, but if Mn exceeds a critical amount ductility and fracture toughness decrease due to the enhancement of the nucleation and growth process.

The void growth rates in the low Mn alloys are 16μm per unit strain and for #4 underaged alloy it is 34μm per unit strain and for #4 overaged alloy it is 75μm per unit strain. The higher values for #4 alloy are due to joining of more closely spaced voids at particles.

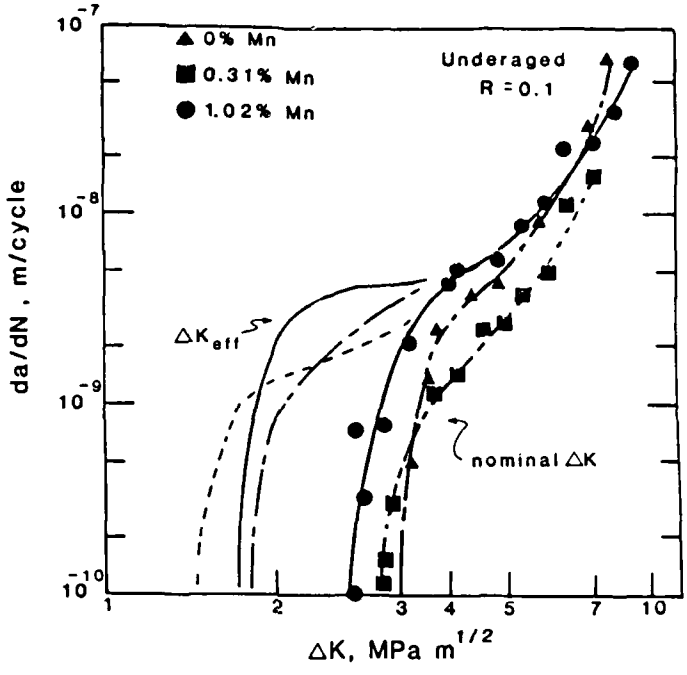

Figure 7: Comparison of fatigue crack growth rates (da/dn) as a function of nominal and effective stress intensity range for different Mn levels in the underaged condition (R=0.1).

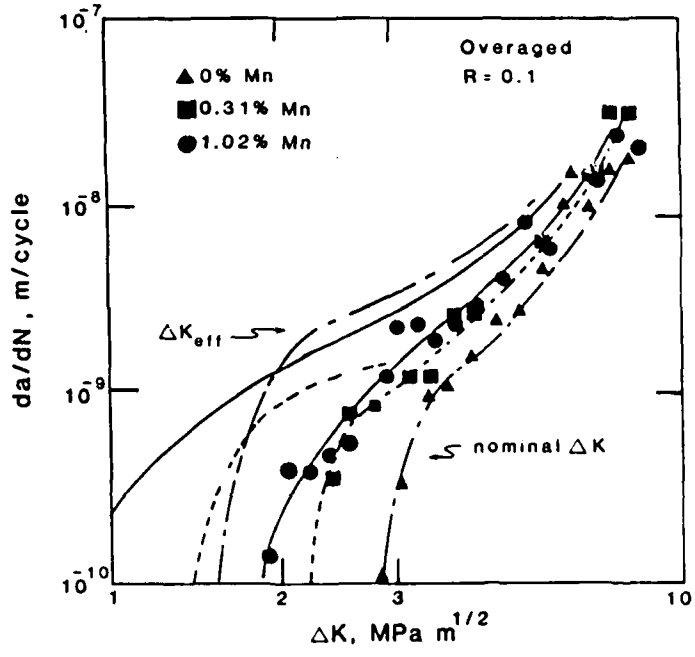

Figure 8: Comparison of fatigue crack growth rates as a function of nominal and effective stress intensity range for different Mn levels in the overaged condition (R=0.1).

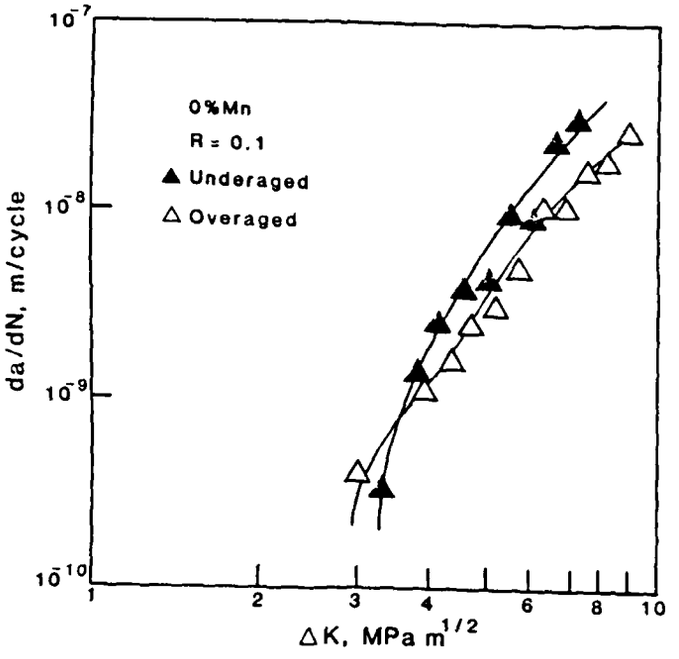

Figure 9: Comparison of fatigue crack growth rates as a function of nominal stress intensity range for a 0% Mn alloy in the under and overaged conditions (R=0.1).

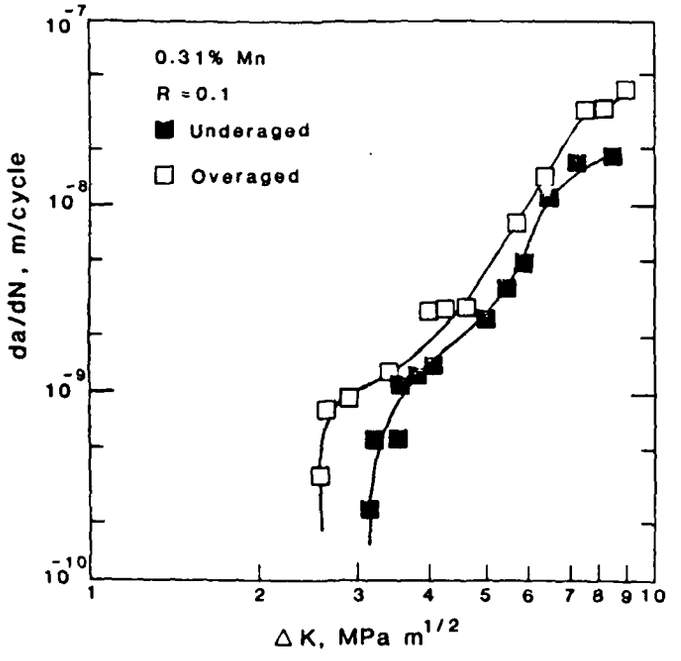

Figure 10: Comparison of fatigue crack growth rates as a function of nominal stress intensity range for 0.3% Mn alloy in the under and overaged conditions (R=0.1).

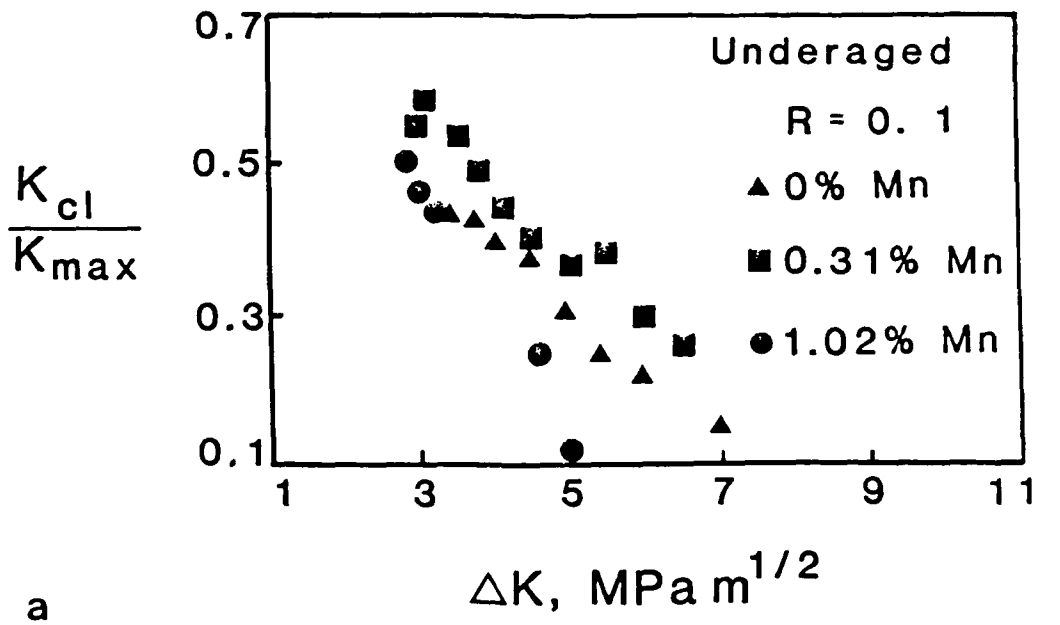

a

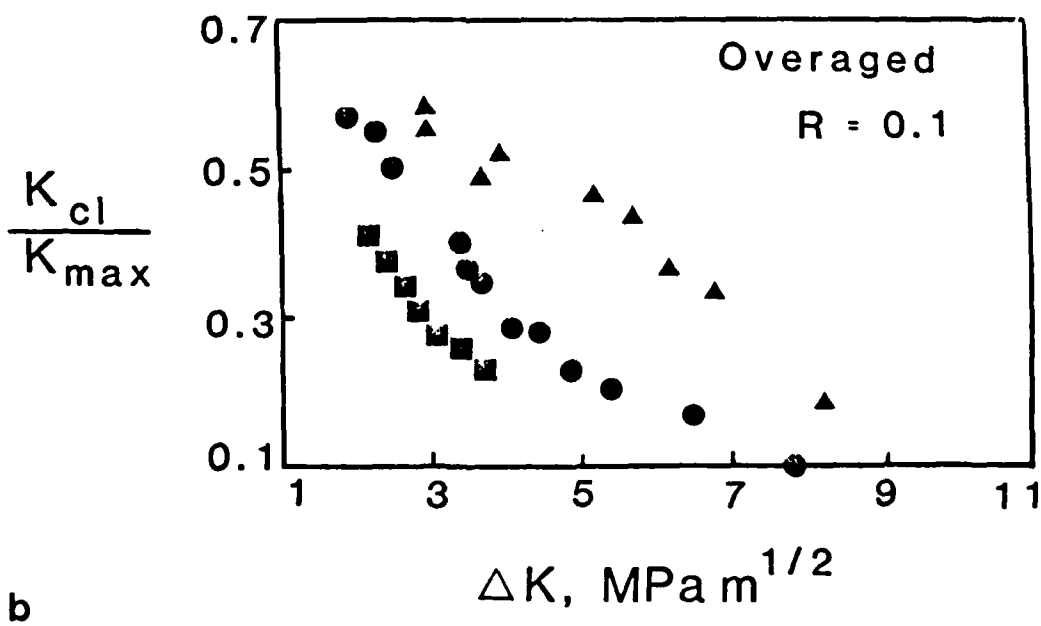

b

Figure 11: Variation of crack closure with nominal stress intensity range in the underaged condition (a) and overaged condition (b).

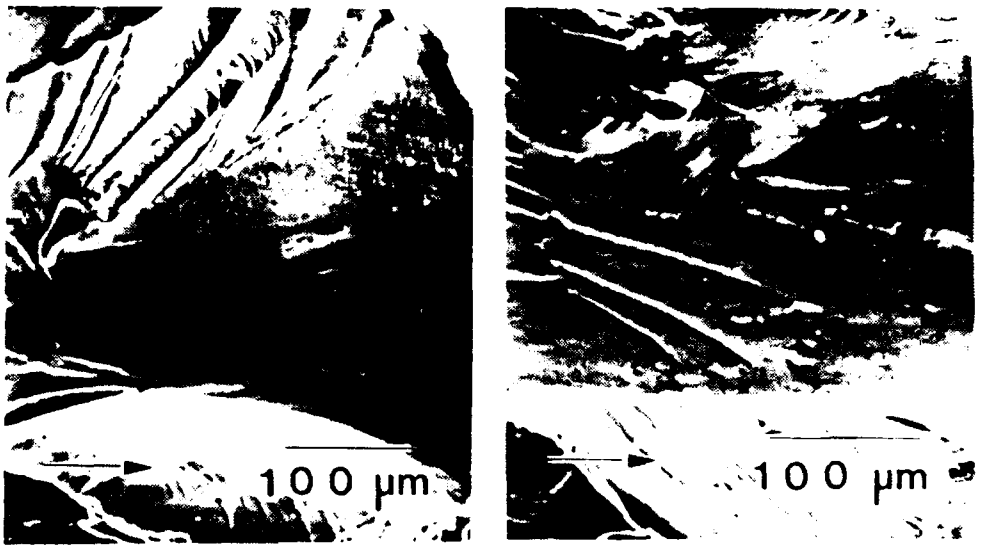

Figure 12: Near-threshold fractographs of overaged alloys 0.0% Mn (a) and 1.02% Mn, overaged alloy (b).

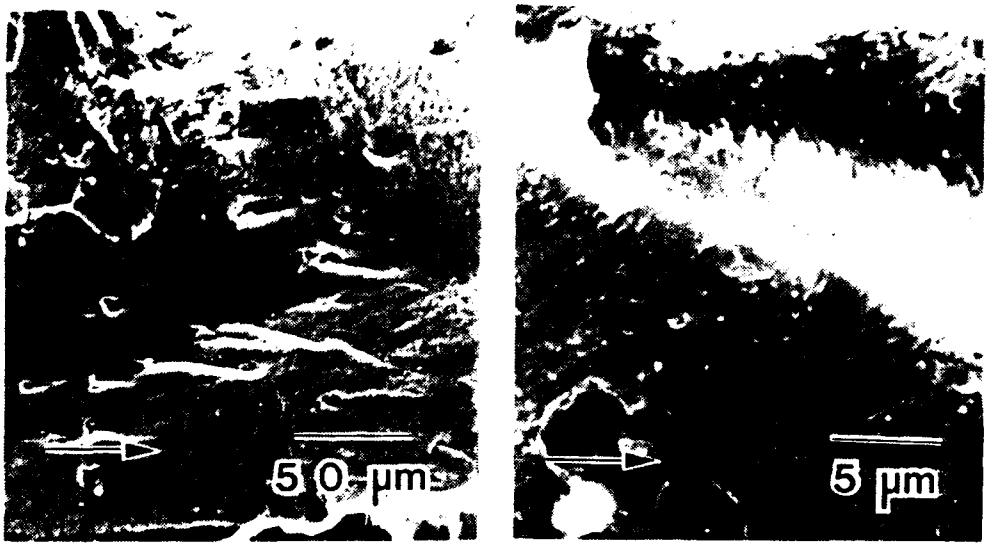

Figure 13: Voids around Mn dispersoids and subsequent striated crack growth in 1.02% Mn, overaged alloy.

The lower ductility levels in the underaged alloys is controlled by void coalescence mechanism along planar slip bands.

1.2 Effects of Mn Rich Particles on Near Threshold Fatigue Crack Growth in 2134 Type Alloys

1.2.1 Summary of Results

The near threshold fatigue crack growth resistance of high purity 2134 type alloys with Zr as the major dispersoid forming element, has been examined in the under and overaged conditons as a function of Mn additions ranging from 0 to 1.02 weight percent at R ratios of 0.1 and 0.5. The additons of manganese resulted in a continuous decrease of the nominal threshold in both the aging conditions with the effect more pronounced in the overaged condition. Crack closure, crack deflections and fractography suggest that roughness induced crack closure is dominant in all alloys. Besides, fractographic evidence suggests that large Mn particles could contribute to local microcrack acceleration resulting in an intrinsic lowering of the fatigue thresholds and faster crack propagation rates.

1.2.2 Dispersoid Effects on Near Threshold Fatigue Crack Growth

Dispersoid forming elements such as Zr, Mn and Cr control the grain structure in aluminum alloys. Additionally Mn and Cr rich particles can homogenize slip and impede slip band impingment at the grain boundaries resulting in a reduced low energy brit ie intergranular fracture. Although these effects could play a role in improving fracture toughness, homogeneous slip might not necessarily improve fatigue threshold behaviour. In precipitation hardened alloys slip reversibilty arguments suggest that homgeneous slip (eg., in the overaged conditions with non shearable particles) reduces the fatigue crack growth

resistance in comparision to inhomogeneous (eg., underaged condition with shearable particles) slip [1,2]. There is however evidence in the literature that Mn dispersoids can substanially improve near threshold fatigue crack growth resistance by supressing intergranular fracture [3]. Results on the effect of Mn additions to Al-Si-Mg alloys show that the fatigue crack resistance in the peak condition is improved due to a decrease in the grain boundary fracture by homogenisation of slip by the Mn rich particles inspite of reduced slip reversibility. Literature on other alloys such as steels suggest that particles such as MnS either do not have any influence on near threshold crack growth rate [4] or could result in an improved fatigue threshold due to crack closure effects. After correcting for crack closure the intrinsic fatigue threshold of alloys containing lower MnS content exhibit higher values [5,6].

A thorough literature search has shown that a systematic evaulvation on the effect of second phase particles on the fatigue threshold behaviour, crack closure, crack deflection, load ratio effects and fractography has not been conducted. The present work was carried out to document the effects of Mn particles on the near threshold fatigue crack growth, crack closure, crack deflections in 2134 type alloys whose grain structure has already been stabalized by Zr. Thus Mn should not have any effect on the grain size and degree of recrystallization. The yield strength of all the alloys was kept approximately the same by choosing appropriate aging times. Both under and overaged conditions were developed to study the effect of the deformation mode on the fatigue threshold behaviour.

1.2.3 Crack Growth Rates

The results obtained from the fatigue crack growth tests conducted in air at a R ratio of 0.1 are shown in Figures 7 and 8 for the under and overaged conditions. In both aging conditions, the effect of Mn is to increase the crack propagation rates at lower ΔK's with the effect more pronounced in the overaged condition. A comparison of the crack propagation rates for any one Mn level show that underaged structures are superior to overaged at near threshold consistent with previous results on under and overaged aluminium alloys (eg. =7), Figures 9 and 10. This is also reflected in the nominal threshold stress intensity factor range for the underaged alloys being higher than the overaged at all Mn levels, Table 5. Fatigue crack growth rates as a function of ΔK at a higher R ratio of 0.5 did not show any significant differences with Mn content. The differences were only observed between the two aging conditions with the underaged again exhibiting superior fatigue crack growth resistance, Table 5. The differences in the crack growth rates between the two R ratios was seen only below delta K of 7 Mpa $m^{\frac{1}{2}}$ suggesting that crack closure played a role in the reduction growth rates at the lower R ratio and at low ΔK levels. Crack closure was observed at 0.1 R ratio and the values are shown in Figure 11. At the high R ratio only the =4 alloy in the overaged condition exhibited crack closure at growth rates of 10^{-10} m/cycle.

Table 5. Fatigue Thresholds

Alloy		Threshold nominal	Threshold effective R=0.1	Threshold effective R=0.5	Mean Crack Deflection	Lineal Roughness Parameter
#1	UA	3.3	2.0	2.2	29	1.14
	OA	3.0	1.34	1.67	14	1.01
#2	UA	3.1	1.85	2.16	25	1.1
	OA	2.4	1.89	1.55		
#4	UA	2.8	1.26	1.85	12	1.02
	OA	1.9	0.93	1.55	16	1.02

1.2.4 Crack Deflections

Crack path profiles of both the under and overaged alloys at lower R ratio were found to be non linear. Since the fracture morphology changed considerably from shear faceted mode at the near threshold to ductile tearing at ΔK's of 5 Mpa-$m^{\frac{1}{2}}$ only the crack deflection angles below this ΔK levels were measured. The results of the mean angle of deflection are shown in Table 5. The lineal roughness values were also measured only below ΔK of 5 Mpa $m^{\frac{1}{2}}$, Table 5. The #1 UA alloy exhibited the highest values of lineal roughness and crack deflection in agreement with the most inhomogeneous slip mode. The trend of these values for other alloys along with the crack closure results, Figure 11, strongly suggest that roughness induced crack closure is dominant in all the alloys tested at R=0.1. This is also supported by the disappearence of closure as well non linearty in the crack path at the higher R ratio (0.5) test.

1.2.5 Fractography

The fracture surface features of the underaged alloys were more crystallographic than the overaged alloys. The crystallographic mode was not significantly affected by the presence of Mn rich particles. However it diminshed in the overaged alloys and more grain

boundary facets were observed. Out of plane cracking was also found to be still prevalent in the overaged conditions. Two near threshold micrographs illustrating the fracture surface asperities, out of plane cracking, grainboundary facet and slipband intersections for alloys #1 and #4 for overaged condition are shown in Figure 12. These features were typical of all the alloys in the overaged condition. In addition to these characterstics the #4 alloy clearly showed larger than average size particles on grain boundary facets interacted with the crack front, Figure 13. In this micrograph trails pointing towards the crack growth direction can be seen. At higher magnifications these trails were associated with either microfacets or striations. When the sample was properly oriented the striations could be clearly observed and the crack growth rate obtained from high magnication shots revealed 1 to 2 orders of magnitude higher crack growth rates than the measured growth rates.

1.2.6 Fatigue Threshold Behaviour

The decrease in ΔK_{th} in the overaged condition for all the alloys can be explained on the basis of reduced non linearity of the crack path and reduced slip reversibilty proposed in the literature [8]. Surface roughness induced crack closure is dominant in all the alloys in both aging conditions. The decrease of the closure level with increasing ΔK level and the disappearence with increasing R ratio [9] support this observation. However crack closure results and fretting corrosion deposits found on fracture surfaces of some alloys suggest that other closure mechanisms may be operating. For instance in the alloy #4 in the overaged condition at R=0.1 crack closure levels were found to be as high as that of #1 alloy. Again the closure persisted at R=0.5,

whereas other alloys did not exhibit this behaviour. This may be due to some contribution to closure arising from the pulled out Mn particles acting as asperities and acting as contact points at levels above K min. Further investigation is necessary before these are ruled out. The fracture surfaces also demonstrated that second phase particles can cause void nucleation at near thresholds. However in low Mn alloys there do not seem to be a clear indication of crack front interaction with the particles or voids. In many cases there was only evidence of slight plasticity around the void. In alloy #4 wherever the fracture was composed of intergranular facets the Mn particles and the associated voids interacted with the crack front.

The present results demonstrate that when sufficently large size and volume fraction of void nucleating particles are present near threshold fatigue crack growth rates could be influenced. In the present study the Mn rich particles which were more equiaxed in the #2 alloy did not seem to have influenced the fatigue threshold behaviour although they were associated with voids. However when the Mn rich particles assumed a more non equiaxed shape the effect was to increase the crack growth rates by local acceleration of the crack front. Striation formation was observed in the vicinity of the cracked particle or void. The creation of the voids in the near threshold region implies that a critical tensile strain is being reached even at these low ΔK levels. Although the overall tensile fracture strain Table 3, is 0.268 the void nucleation tensile strain has been determined to be less than 0.02 to create 0.1 volume percent of voids.

1.2.7 Conclusions

1) The fatigue crack growth rates in 2134 alloys decrease with increasing Mn content. The roughness induced crack closure in all the alloys tested arises from fracture surface roughness. Substantial mode II displacements and fracture surface asperites comparable to the crack tip opening displacement were observed in all cases.

2) Although the highest Mn level alloy exhibited closure levels comparable to the lower Mn alloys the nominal and also the effective fatigue thresholds were lower in the overaged condition.

3) Fractography suggests that in the highest Mn level alloy there is a crack front particle interaction which causes local faster crack propagation. The regions near the Mn particles exhibited striations which showed 1 to 2 orders of magnitude higher crack growth rates than the macroscopic or measured growth rates.

1.2.8 References

1. E. Hornbogen and K.H. Zum Gahr: Acta Metall. 24, 1976, p. 581.

2. R.D. Carter, E.W. Lee, C.J. Beevers and E.A. Starke: Metall. Trans. A 15A, 1984, p. 555.

3. L. Edwards and J.W. Martin: Metal Science 17, 1983, p. 511.

4. G.J. Fowler: Mater. Sci. and Engg. 39, 1979, p. 121.

5. A.J. Cadman: C.E. Nicholson and R. Brooks, paper #34, International Symposium on Fatigue Thresholds, Stockholm, Sweden, June 1981.

6. A.D. Wilson: Fracture: Interactions of Microstructure, Mechanisms, Mechanics, eds. J.M.Wells and J.D.Landes, AIME, 1984, p. 235.

7. K.V. Jata and E.A. Starke: Metall. Trans. A 17, 1986, p. 1011.

8. S. Suresh: Metall.Trans. A 16A, 1985, p.249.

9. S.Suresh and R.O.Ritchie: Metall.Trans. A 13A, 1982, p. 1627.

10. J.A. Walsh, K.V. Jata and E.A. Starke: 1986, TMS Fall Meeting, Orlando, Florida, USA.

Part 2. Intergranular Fracture of Al-Li-Base Alloys

J. A. Wert, P. Bourgasser, and E. A. Starke, Jr.

Abstract of Part 2

Part 2 of this investigation has examined intergranular fracture during heat treatment and deformation of an Al-Li-Cu alloy and an Al-Li-Cu-Mg alloy. When the Al-Li-Cu-Mg alloy used in this study is solution treated by rapid heating to 550°C, nonequilibrium eutectic melting of a soluble phase occurs. The liquid spreads along grain boundaries as a thin film, which solidifies by diffusion of solute into the adjoining grains. Upon quenching, intergranular cracks are found at grain boundaries where a liquid film had formed during solution treatment. At solution treatment temperatures of 530°C and below, nonequilibrium eutectic melting did not occur and no intergranular cracks were found in as-quenched specimens. The eutectic melting is associated with a soluble precipitate phase. No evidence of nonequilibrium eutectic melting was found in the companion Al-Li-Cu alloy.

For the Al-Li-Cu-Mg alloy, intergranular fracture occurred during tensile testing of as-quenched and quenched-and-aged specimens, irrespective of whether nonequilibrium eutectic melting had taken place during solution treatment. For the Al-Li-Cu alloy, intergranular fracture occurred during tensile testing of quenched-and-aged specimens, but not of as-quenched specimens. The cause of intergranular fracture during deformation of these alloys is unlikely to be segregation of Na and K impurities to grain boundaries. Several additional explanations for intergranular fracture have previously been proposed, but the available evidence in the present case does not strongly support or exclude any of the remaining explanations.

Part 2. Intergranular Fracture of Al-Li-Base Alloys

2.1 Introduction

Recent studies of Al-Li-Cu and Al-Li-Cu-Mg alloys have shown that these alloys can exhibit intergranular fracture [1-14]. The most commonly-observed manifestation of this intergranular fracture is appearance of secondary cracks on fracture surfaces of tensile specimens loaded parallel to the rolling direction. In addition, tensile elongation in the short transverse orientation is severely degraded by intergranular fracture [5]. This phenomenon is of relatively minor importance in sheet products because sheet is rarely loaded in the short transverse direction. However, plate and extruded products are frequently loaded in the short transverse direction, and poor grain boundary cohesion would be a limiting factor in many applications.

The intergranular fracture phenomenon is particularly notable because Al-Li-base alloys of commercial compositions are usually unrecrystallized after hot rolling to final gauge. Consequently, the grains are large, and they become quite elongated during hot rolling. It is not unusual to find an average grain intercept length larger than 1 mm in the longitudinal direction. These long boundaries become planes of weakness when the material is loaded in the short transverse direction.

Since intergranular fracture of unrecrystallized Al-Li-Cu(-Mg) alloys poses a barrier to wide use of these alloys in aerospace applications, investigators in the US and Western Europe have studied this problem. Based on these prior investigations, explanations for the origin of intergranular fracture in Al-Li-Cu(-Mg) alloys have been proposed [1-14]. These explanations fall into 4 broad categories:

i. stress concentration at grain boundaries due to planar slip,
ii. strain localization in precipitate free zones (PFZs),

iii. stress concentration at grain boundary precipitate particles, and
iv. segregation of Na and K impurities to grain boundaries.

At the outset of this investigation, we sought to answer 2 fundamental questions:

1. Which intergranular fracture mechanisms are most important in commercial-type Al-Li-Cu(-Mg) alloys?
2. What can be done to reduce or eliminate this type of fracture?

Results of the investigation are described in the following sections of this report. The principle result has been discovery of a fifth mechanism which can produce intergranular fracture in Al-Li-Cu-Mg alloys, nonequilibrium eutectic melting of grain boundary phases during solution treatment. Since this investigation focussed on two alloy compositions, it is not clear what proportion of Al-Li-base alloys are susceptible to intergranular fracture due to nonequilibrium eutectic melting.

2.2 Experimental Procedure

2.2.1 Alloys: Composition and Primary Processing

The alloys investigated in this study were supplied by Reynolds Metals Co. They were DC cast in the form of ingots with a 168 mm x 81 mm cross-section. After casting, they were homogenized 24 hr. at 543°C and hot rolled to 12.7 mm thick plate, which represents a 84% reduction ratio. Cross-rolling was used during initial break-down of the ingots, to provide a final plate of the desired dimensions. Reynolds Metals Co. also supplied pieces of the ingots, which permitted characterization of the cast structure and of changes that occurred in the structure during homogenization and hot rolling.

The result of the chemical analysis of these two alloys, performed by Luvak Inc., is given in Table 2.1.

Table 2.1

Alloy Composition (Wt. %)

	LC1	LCM1
Li	2.45	2.46
Cu	2.43	2.04
Mg	.003	.96
Zr	.18	.14
Fe	.098	.11
Si	.089	.047
Na	.0014	.0006
K	.0005	.0005
Ca	<.0005	<.0005

The Reynolds casting reference number is 59373 for LC1 and 59379 for LCM1. According to the International Aluminum Association code, LC1 is an AA2090 alloy, and LCM1 is an AA8091 alloy.

2.2.2 Metallographic Methods

Specimens were ground on grit paper before diamond paste polishing and final Mastermet polishing. Grain structure was revealed by Keller's reagent. The cast grain structure was revealed by anodizing the alloys in Barker's solution and using polarized light for microscopic observation.

2.2.3 X-Ray Diffraction

Pinhole back-reflection and pole figures techniques were used to determine the extent of recrystallization during hot rolling. Samples of both alloys were solution heat treated, mechanically polished (600

grit), etched 2 min. in sodium hydroxide at 70°C and cleaned in dilute nitric acid before pole figure determination was performed. The same samples were used for pinhole back-reflection experiments. Pole figures were obtained using a Siemens back-reflection texture goniometer. Cu K_α radiation was used.

2.2.4 Heat-Treatment

The alloys were solution-heat-treated (SHT) in a salt-bath at temperatures between 500 and 550°C and water-quenched at room temperature. They were aged in an oil-bath or in a convection air-furnace at 170 or 190°C.

2.2.5 Hardness Testing

Rockwell-B hardness was measured to determine the aging response of the alloys at the temperatures indicated above. Specimens were ground on 600-grit paper prior to testing and a load of 100 kg was used to perform the hardness tests.

2.2.6 Tensile Testing

Tensile tests were performed on an MTS-series 810 system, using an extensometer to measure elongations. The initial strain rate was 10^{-3} s^{-1}. Round tensile specimens were used in most cases; but smaller, flat specimens had to be used for thermomechanically processed materials.

2.2.7 Fractography

A JEOL JSM-35 Scanning Electron Microscope (SEM) was used for the examination of fracture surfaces. Measurements of fraction of cracked grain boundaries were performed on optical micrographs of the LS plane from fractured tensile specimens.

2.2.8 Transmission Electron Microscopy

The Transmission Electron Microscope (TEM) investigation was performed on a Philips EM 400-T. Samples were prepared by electropolishing 3 mm discs in Tenupol-2 twin-jet apparatus at 13 V DC using a 3:1 methanol:nitric electrolyte cooled to -15°C.

2.2.9 Recrystallization Treatment

A special thermomechanical process (TMP) was used to recrystallize the alloys. It consisted of:

- SHT of 30 min. at 530 or 550°C
- aging 8 hr. at 450°C and, in most cases, 8 hr. at 350°C
- hot rolling: 80% reduction at 250 or 300°C
- recrystallization: 1 hr. at 530 or 550°C.

2.3 Results and Discussion

2.3.1 Microstructure of As-Received Materials

Since this study examined intergranular fracture, it was essential to determine whether the alloys recrystallized during either hot-rolling or subsequent SHT. Both alloys exhibit a typical pancake grain morphology. Figure 1 shows the microstructure in all three orientations. The Mg-containing alloy, LCM1, has a coarser grain structure.

Samples from the ingots allowed characterization of the microstructure of the alloys in the cast condition (before homogenization). Figure 2 shows the cast microstructures. The plane of the photographs is normal to the casting direction and the location is approximately at the center of the ingot cross-section. Little difference was found in grain size from the edge to the center of the castings.

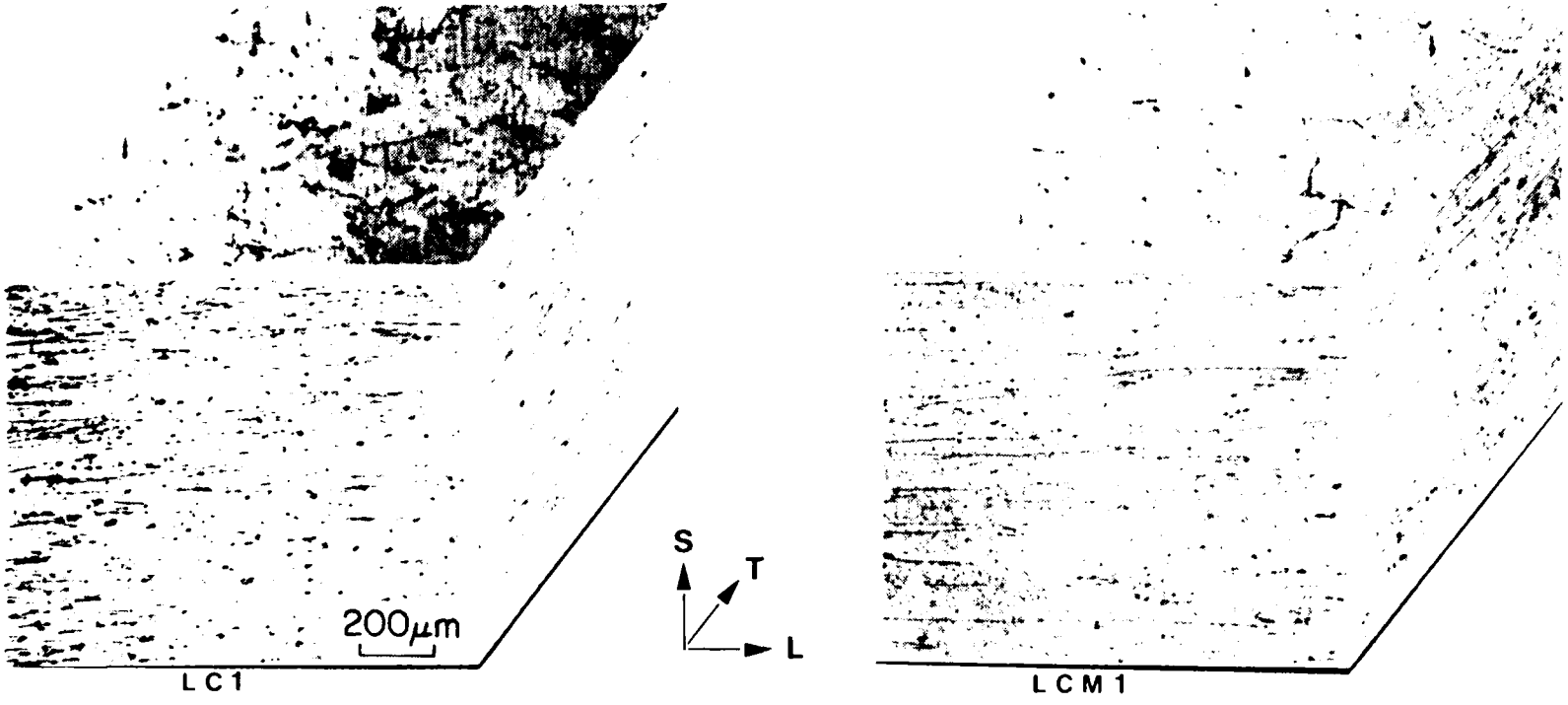

Fig. 1 Optical micrographs showing grain structure of alloys LC1 and LCM1. Solution treated 15 min. at 530°C and quenched.

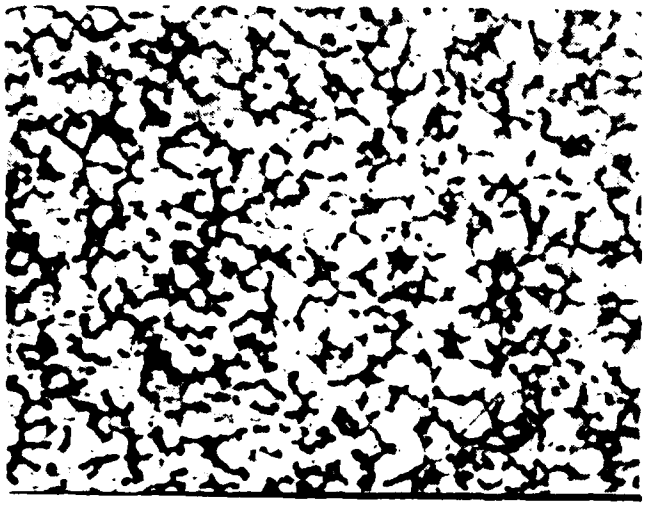

a: LC1, Keller's etch

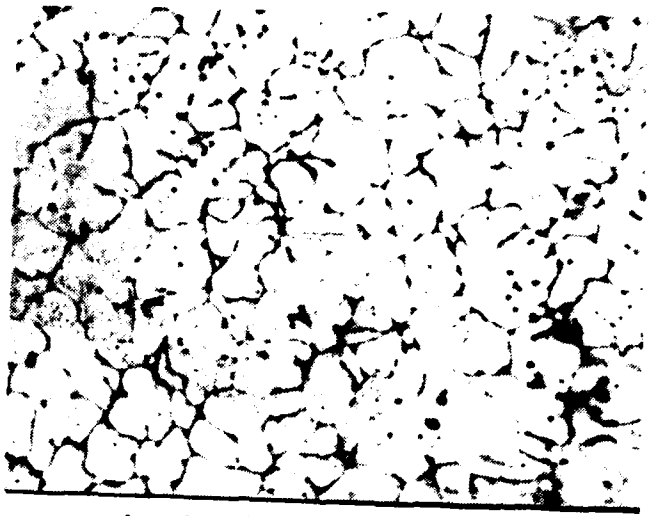

b: LCM1, Keller's etch

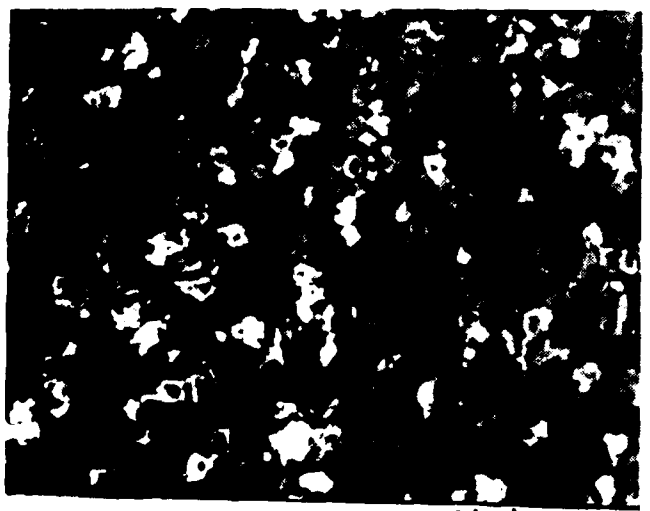

c: LC1, Barker's anodizing

d: LCM1, Barker's anodizing

Fig. 2 Optical micrographs showing as-cast grain structures of alloys LC1 and LCM1.

These cast structures are typical of grain-refined, DC-cast aluminum alloys. The cast grain size cannot be determined from Figures 2a and 2b because the grains do not have sufficient contrast. Additional micrographs, shown in Figures 2c and 2d, were taken following anodizing. They allowed the grain sizes in the castings to be determined.

Knowing the cast grain size and the extent of rolling reduction, the final grain size can be calculated assuming no recrystallization occurred during hot rolling. Results of these calculations are shown in Table 2.2. The calculated and measured short transverse grain sizes compare favorably, leading us to the conclusion that recrystallization did not occur during hot rolling.

Table 2.2
Prediction of Grain Size After Hot Rolling

Alloy	As-Cast μm	Hot-Rolled Predicted μm	Hot-Rolled Observed μm
LC1	130	21	18
LCM1	370	58	40

A surprising feature of the cast structures is the difference in dendrite spacing and grain structure in two nominally-identical castings. Dendrite spacing is usually determined by cooling rate. The difference in structure thus suggests a rather large difference in cooling rate of these two alloys. However, Reynolds Metals Co., producer of this material, is confident that the cooling rates were approximately equal for these two castings. The origin of the grain size difference is not presently known. Although the grain size of the

casting is reflected in the hot-rolled microstructure, this difference is not thought to pose substantial problems in interpreting the results of the present study.

X-ray investigation provided additional evidence for the absence of recrystallization during hot working. The <111> pole figures for both alloys, shown in Figure 3, are typical of rolled aluminum alloys. Evidence of cross-rolling during hot rolling of the ingots can be seen in the pole figures [15,16]. The pole figures support the conclusion that no recrystallization occurred during the final rolling steps or during subsequent solution treatment. Pinhole back-reflection photographs showed essentially continuous rings rather than individual reflections, confirming the presence of a deformation substructure in both alloys.

2.3.2 Transmission Electron Microscopy

Electron microscopy of solution treated and quenched sampled enabled characterization of the grain and subgrain structure of alloys LC1 and LCM1. The elongated grain structure found by optical microscopy was also apparent in TEM specimens. In addition, a subgrain boundary network was observed within the elongated grains, with an average subgrain diameter of about one third of the short-transverse grain dimension. This subgrain structure, found by previous investigators in similar alloys [17,18], is the result of recovery during hot rolling. Subgrain boundaries are free of precipitation after SHT, but grain boundaries exhibit some precipitates in the alloy LCM1.

Grain interiors have been found to contain Al_3Li, Al_3Zr and constituent particles similar to those found at grain boundaries. The dispersion of Al_3Li was very fine in the unaged samples, as is expected

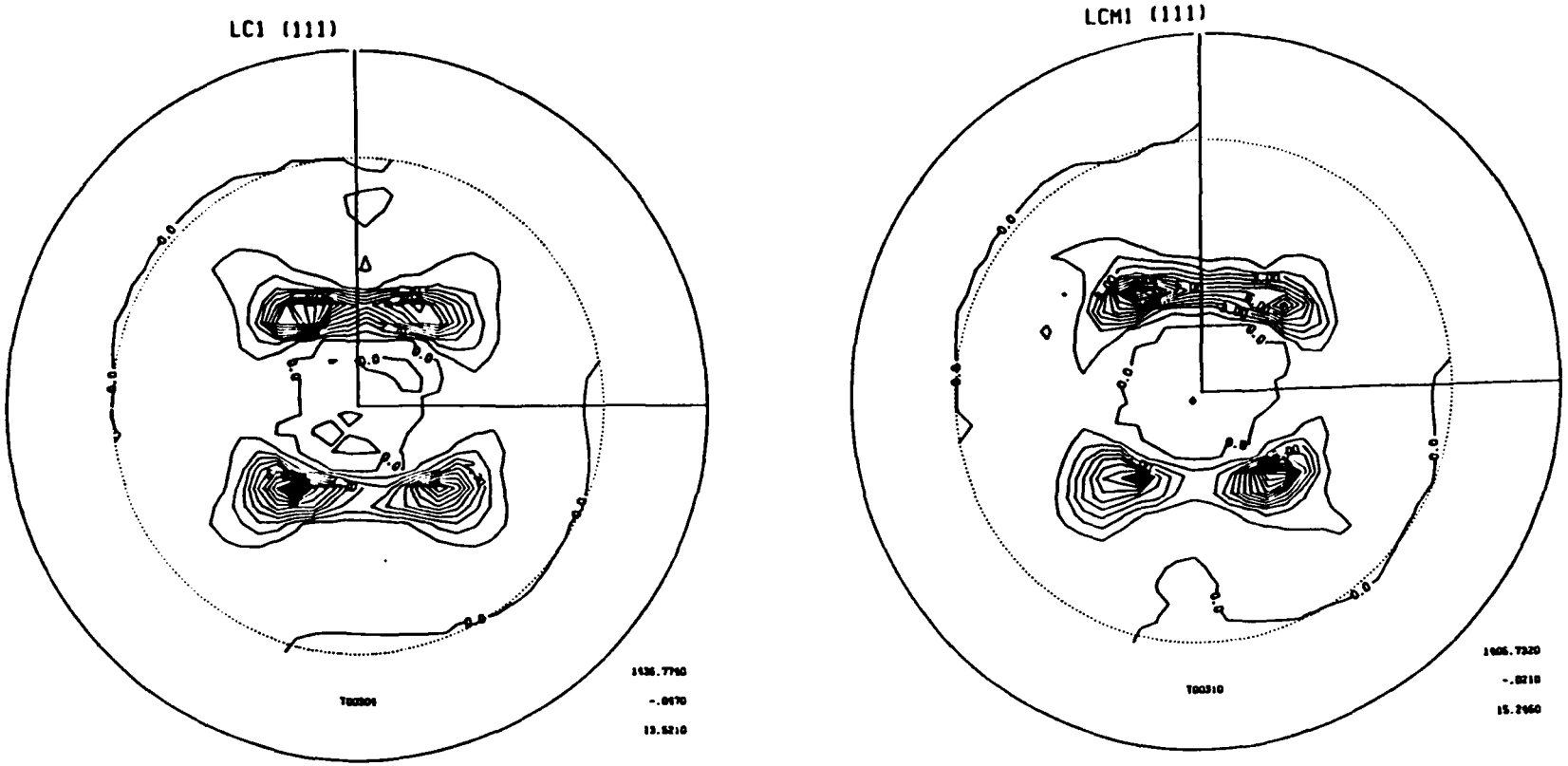

Fig. 3 <111> pole figures of alloys LC1 and LCM1.

for precipitates that form during quenching. The inability to suppress Al_3Li by conventional quenching procedures has been noted by previous investigators [17,18]. The Al_3Zr particles were found to have an average diameter of 7 nm, typical of many other aluminum alloys containing Zr.

TEM was performed on aged specimens, in an effort to identify precipitates that form during aging. Figure 4 compares grain and subgrain boundaries in underaged and peak-aged conditions for alloy LC1. Figure 4a, an underaged condition, shows only small grain boundary precipitates and light T_1 precipitation within the grains. In contrast, Figure 4b which corresponds to a peak aged condition reveals fairly large grain boundary precipitates (as large as 0.5 μm) and a 0.5 μm-wide T_1 precipitate free zone along grain and subgrain boundaries. The large precipitates on grain boundaries in alloys LC1 and LCM1 have been identified by other studies [19,20] as the icosehedral phase T_2.

2.3.3 Solution Heat Treatment Temperature

2.3.3.1 Solution Treatment Temperature Based on Complete Solutionizing

Specimens of both alloys were first solutionized at 530°C for 15 minutes. The metallographic study showed the presence of some particles after this treatment; these were identified as undissolved precipitates. A concurrent study conducted at Reynolds showed that solutionizing at 530°C does not provide maximum strengthening, and suggested that a temperature of 543 ± 5°C should ensure adequate solutionizing without melting for both alloys [16].

a: aged 48 hr. at 170°C

b: aged 192 hr. at 170°C

Fig. 4 TEM micrographs showing the effect of aging on the microstructure of alloy LC1 solution treated 30 min. at 530°C. a) Aged 48 hr. at 170°C. b) Aged 192 hr. at 170°C.

Therefore, additional samples were solutionized at 550°C for times of 15 min., 30 min. and 1 hr. These experiments showed that SHT of 15 min. or more at 550°C completely dissolves all soluble precipitates.

2.3.3.2 Effect of Solution Treatment Temperature on Intergranular Fracture

After using the 550°C SHT temperature for for heat treatment of a set of tensile specimens, we found that alloy LCM1 exhibited grain boundary cracks in the solution-treated condition -- before tensile testing. An example of intergranular fracture in LCM1 after SHT at 550°C is shown in Figure 5. A metallographic sample of the same alloy solutionized at 530 did not show any cracks. Neither did a sample maintained at 530°C and heated to 550°C at a rate of 20°C/hour.

Transmission electron microscopy (TEM) specimens were prepared from the quenched samples of alloy LCM1 in an effort to further characterize the nature of the intergranular cracks. Figure 6 shows the morphology of the grain boundary in a location where an intergranular crack extended into the edge of the foil. The schematic diagram in Figure 6a shows the overall geometry of this specimen, while the TEM micrograph shows the detailed morphology of the grain boundary just beyond the crack tip. It is evident from the bright field micrograph that a phase is interposed between the two grains. Electron diffraction confirmed that this grain boundary phase has an fcc crystal structure with a lattice parameter indistinguishable from that of the matrix grains. Diffraction experiments also confirmed that the phase between the two aluminum grains has a different lattice orientation than either of the neighboring grains.

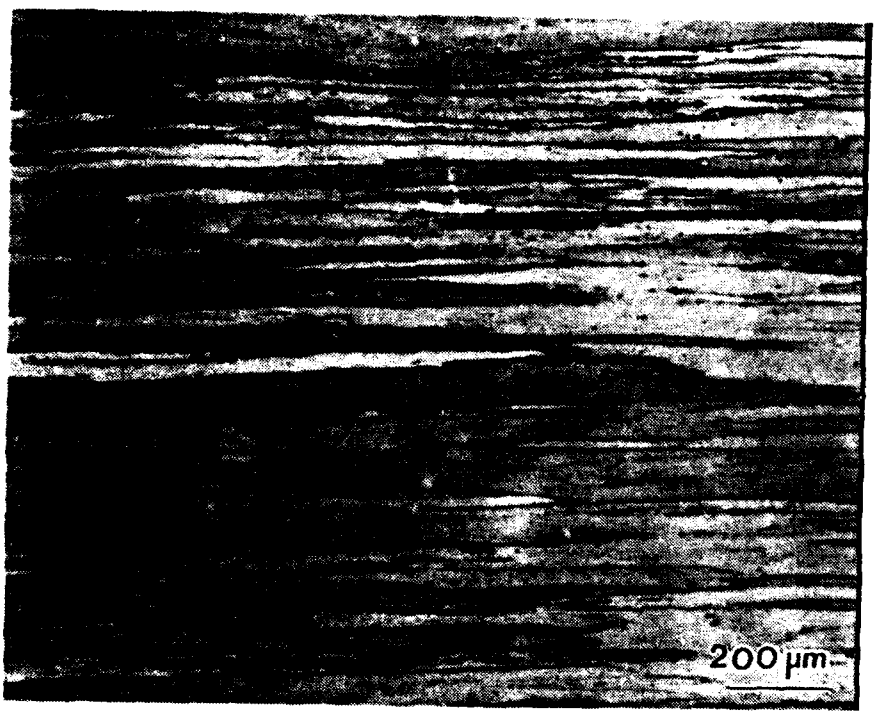

Fig. 5 Optical micrograph showing intergranular fracture of alloy LCM1 after solution treatment at 550°C.

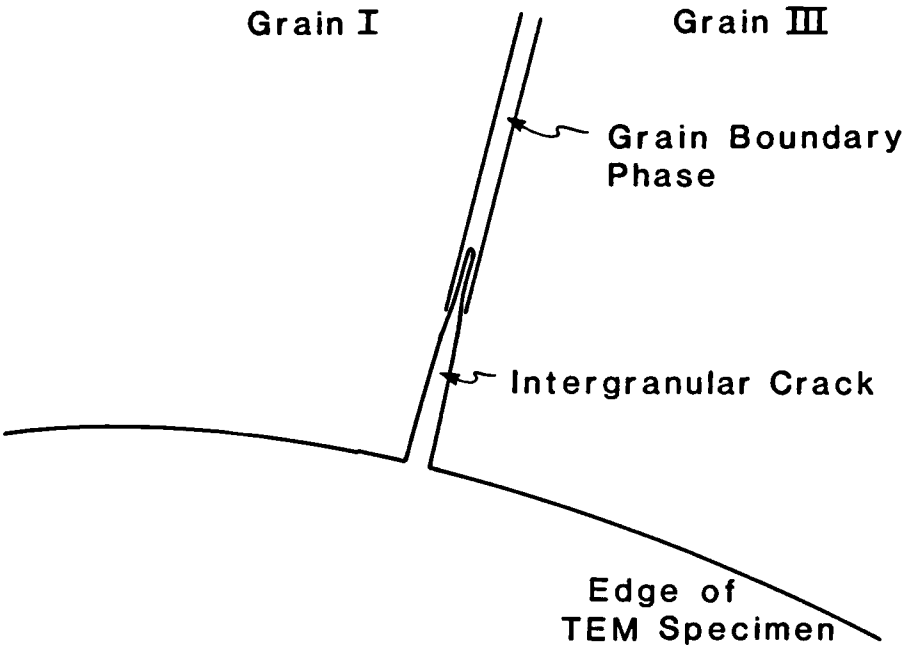

Fig. 6a Schematic of TEM specimen.

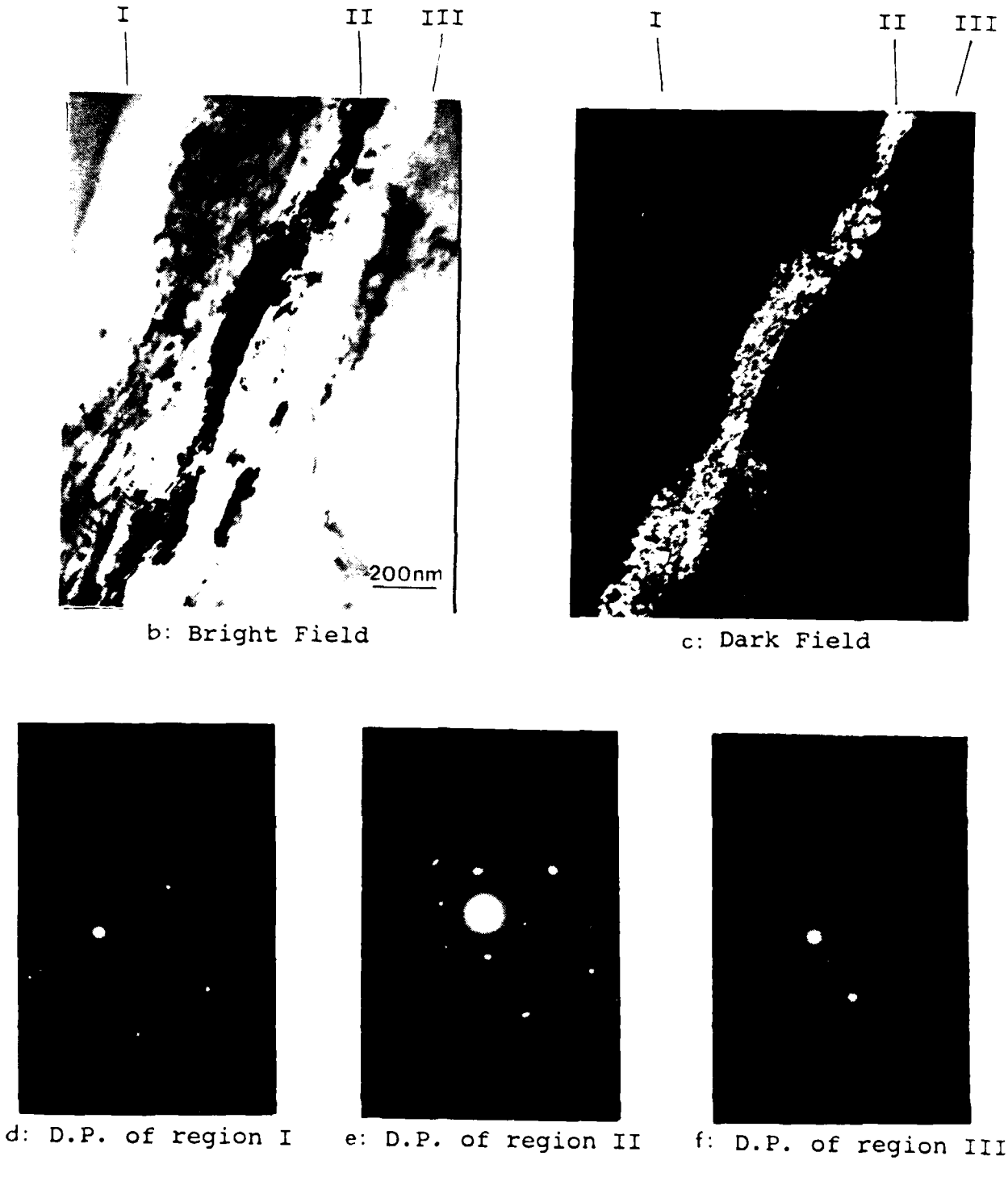

Fig. 6b-f TEM micrographs showing grain boundary phase in alloy LCM1 after solution treatment at 550°C. b) Bright field micrograph of grain boundary phase. c) Dark field micrograph of grain boundary phase. d)-f) Diffraction patterns from regions I-III.

Similar TEM observations of intergranular cracks were made in other thin foils taken from specimens of alloy LCM1 solution treated at 550°C. In every case where an intergranular crack was observed in a TEM specimen, the intergranular phase with the same crystal structure and lattice parameter as the matrix phase was present along the grain boundary which had fractured. Grain boundaries which had not fractured did not contain the grain boundary phase.

TEM specimens were prepared from quenched samples of alloy LCM1 solution treated at 530°C and from alloy LC1 solution treated at 550°C. No cracks were found in the TEM specimens and the grain boundary phase was not observed.

Several TEM specimens were prepared after shorter solution treatments in an attempt to observe undissolved grain boundary particles in conjunction with the grain boundary phase. In one case, an undissolved particle with a diameter of approximately 2 μm was found at a grain boundary where the grain boundary phase was present. Energy dispersive X-ray analysis of this particle showed that it contained Al and Cu in a ratio of approximately 2:1. This particle did not contain Mg, but its Li content is uncertain because Li is not detectable by EDS methods. The grain boundary particle was too large to permit electron diffraction information to be obtained.

Interpretation of these experimental observations is described in section 2.4 of this report.

2.3.4 Aging Response from Hardness Results

Aging response curves at 170 and 190°C for alloys LC1 and LCM1 are shown in Figure 7. At 170°C, the aging curve shows only

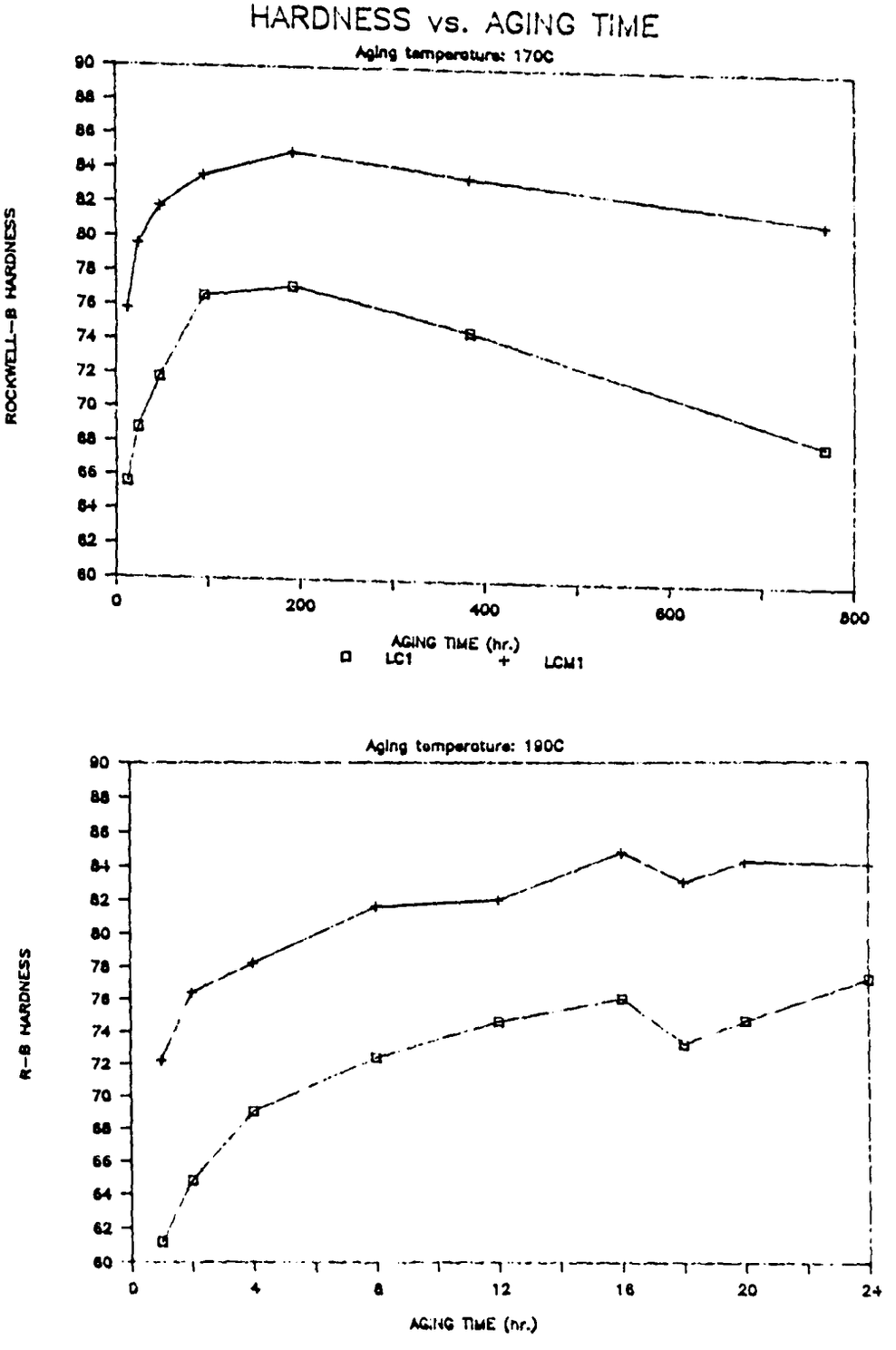

Fig. 7 Hardness vs. aging time for alloys LC1 and LCM1. Both alloys solution treated at 550°C. a) Aged at 170°C. b) Aged at 190°C.

one peak, after 192 hr. of aging. This time was chosen as peak-aging time at 170°C.

At 190°C, there is an increase of hardness from 0 to 16 hr., followed by a decrease from 16 to 20 hr. and a second increase after 20 hr. An concurrent study being conducted at the University of Virginia showed the same type of evolution for elastic modulus of alloy LC1 aged at 190°C [19]. It is believed that the first increase is due to precipitation/growth of T_1 and δ'. The decrease is thought to be due to precipitation of T_2, the icosehedral phase observed in Al-Li-Cu-(Mg) alloys [21-23]. The reason for the second increase is unknown at this day. An aging time of 16 or 24 hr. was chosen for peak-age at 190°C.

2.3.5 Tensile Test Results

Tensile properties of alloys LC1 and LCM1 were measured as a function of solution treatment temperature and of aging time at 170°C. This aging temperature was selected because it is sufficiently low to postpone precipitation of grain boundary phases in many types of Al-Li-Cu-(Mg) alloys [17,18]. Figure 8 shows the variation of the 0.2% offset yield strength and the tensile strength as a function of aging time after solution treatment of both alloys at 550°C. Both alloys achieve peak strength for an aging time near 200 hours at 170°C. Figure 8 also shows the variation of the elongation to failure with aging time.

Since solution treatment of alloy LCM1 at 550°C produces intergranular cracks without application of an external stress, tensile properties were measured as a function of solution treatment temperature for as-quenched specimens. The table comprising Appendix 2.1 contains the results of these tests, which reveal that presence or

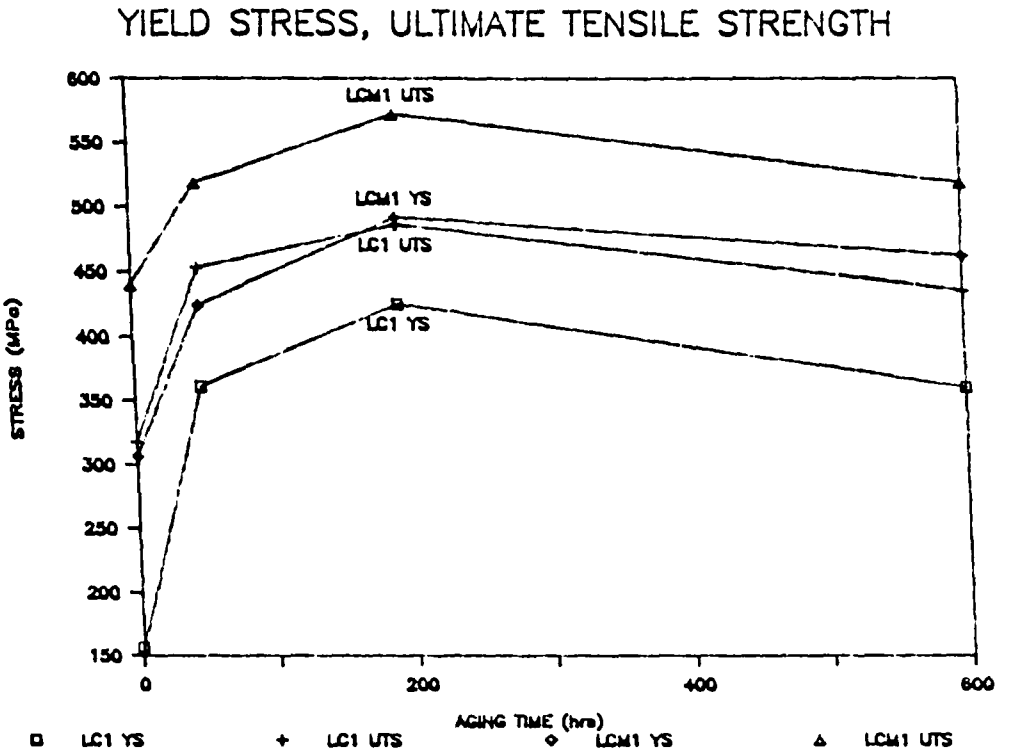

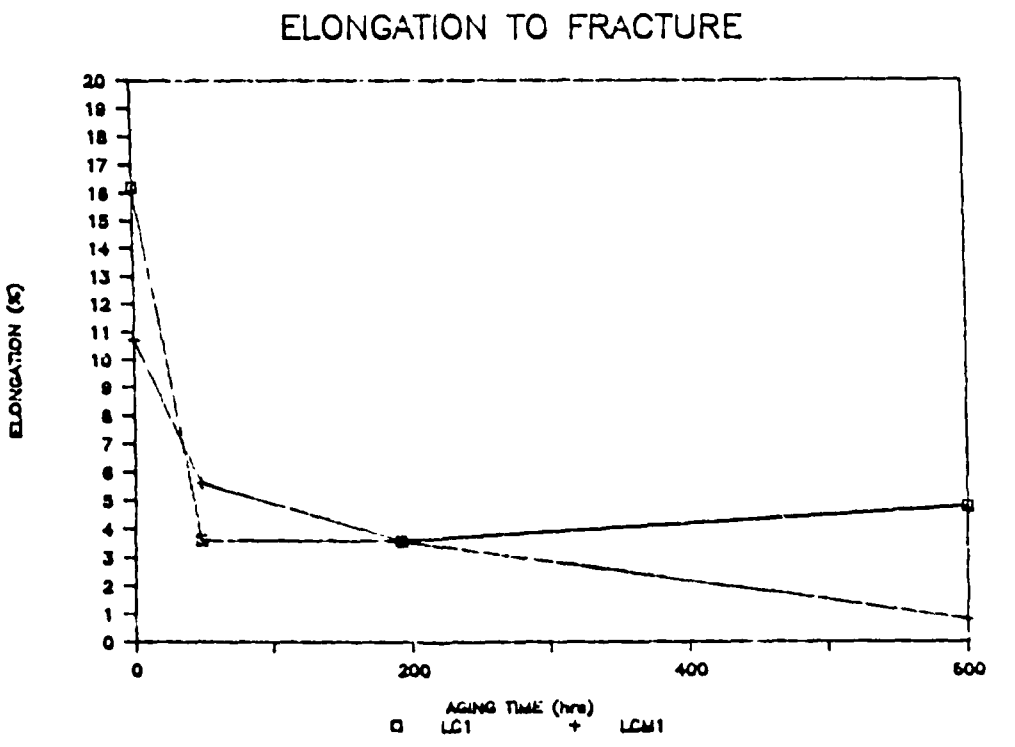

Fig. 8 Tensile properties vs. aging time for alloys LC1 and LCM1. Both alloys solution treated at 550°C. a) Aged at 170°C. b) Aged at 190°C.

absence of intergranular cracks prior to testing does not influence the elongation to failure in alloy LCM1.

Additional tensile test results for specimens solutionized 30 min. at 550°C and aged at 190°C, and for specimens solutionized at 530°C were also tested are contained in Appendix 2.1.

2.3.6 Fractography

Figure 9 shows the type of fracture surface found for both of alloy LC1 and alloy LCM1 for nearly all aging conditions. Intergranular fracture is manifested by deep secondary cracks on the surface of the longitudinal tensile specimens, with transgranular fracture found between the secondary cracks. Such fracture features are characteristic of unrecrystallized Al-Li-Cu-(Mg) alloys tested with the tensile axis parallel to the rolling direction [17,18].

The only exception to this fracture surface topology was found on as-quenched specimens of alloy LC1. In this case, the secondary cracks did not appear, indicating that intergranular fracture had not occurred during tensile deformation.

2.3.7 Metallography of Failed Tensile Specimens

To further understand the nature of the intergranular cracking behavior in alloys LC1 and LCM1, failed tensile specimens were sectioned parallel to the LS plane after straining to failure. Metallographic examination of the microstructure below the fracture surface was then conducted. An example of one such specimen is shown in Figure 10. These observations confirmed that secondary secondary cracks on the fracture surface represent intergranular fracture in both alloys.

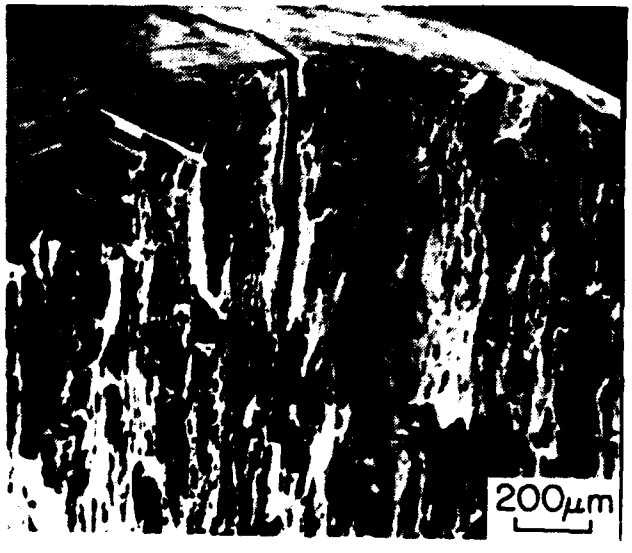

Fig. 9 Secondary intergranular cracks on fracture surface. Alloy LCM1 SHT 30 min. at 550°C, aged 48 hr. at 190°C.

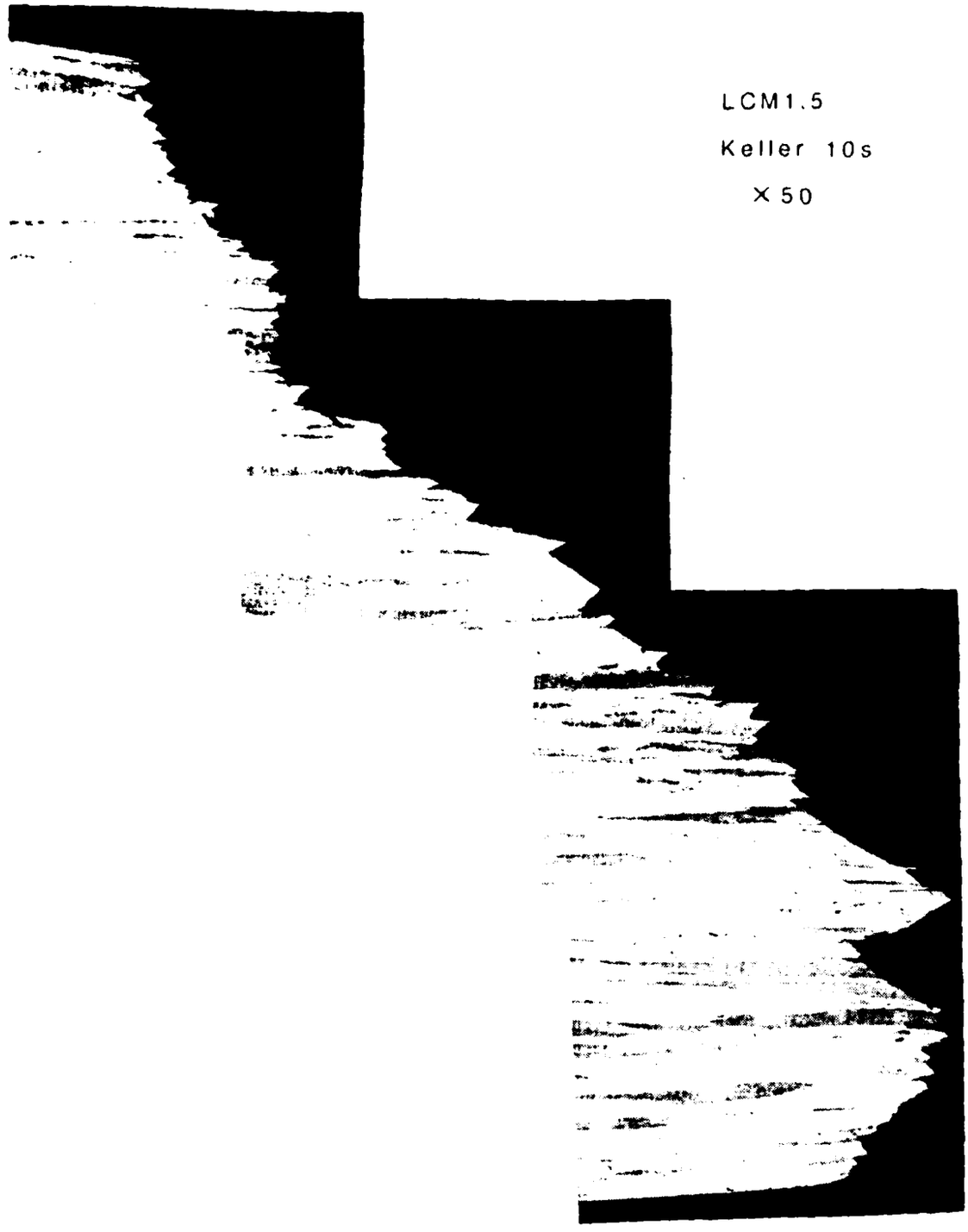

Fig. 10 Sectioned tensile specimen after testing to failure. Alloy LCM1 SHT 30 min. at 550°C, aged 48 hr. at 190°C. (TS plane)

Part 2. Intergranular Fracture of Al-Li-Base Alloys

The propensity for intergranular fracture during longitudinal tensile straining was assessed by determining the fraction of cracked grain boundaries (f_C) across the width of the tensile fracture surface. Grain boundaries that produced either a secondary crack or a fracture plane parallel to the loading axis were counted as fractured boundaries. Results of these measurements are shown in Figures 11a and 11b where the fraction of grain boundaries producing an intergranular fracture during tensile deformation is shown as a function of solution treatment temperature (11a), and as a function of aging time after solution treatment at 550°C (11b). This type of quantitative assessment of the extent of intergranular fracture in Al-Li-base alloys has not previously been reported.

The results in Figure 11a show that the fraction of fractured grain boundaries after tensile testing of as-quenched specimens is independent of solution treatment temperature. Thus, even though alloy LCM1 exhibited intergranular fracture before tensile testing when solution treated at 550°C, but not at 530°C or below; f_C after tensile testing was independent of solution treatment temperature.

The results obtained by this methods allow us to conclude that aging promotes intergranular fracture in both alloys. This is particularly noticeable in LC1 where no intergranular fracture occurred in solutionized materials. The curves also establish that lowering the SHT from 550 to 530 or 500°C does not reduce significantly secondary cracking after tensile testing in alloy LCM1, despite the cosiderable difference in the extent of intergraular fracture prior to testing. It is noticeable from comparison of Figures 8 and 11 that an underaging

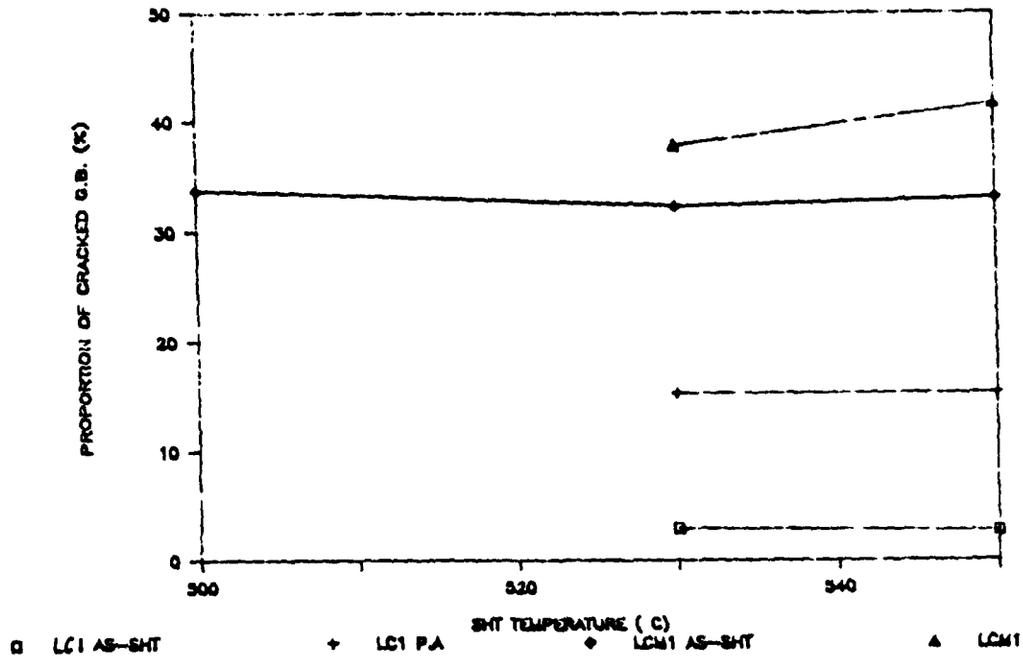

a: Influence of solutionizing temperature. Solutionizing time: 30 min. As-solutionized and peak-aged conditions

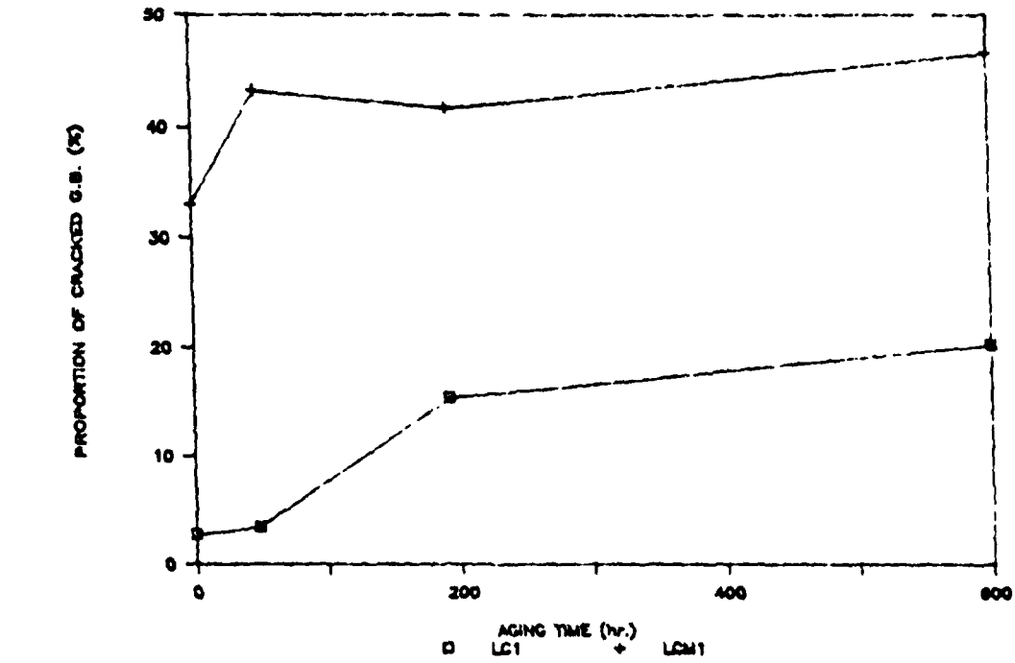

b: influence of aging time. Aging temperature: 170°C.

Fig. 11 Effect of solution treatment temperature and aging time in secondary intergranular fracture. a) Fraction of cracked grain boundaries as a function of solution treatment temperature. b) Fraction of cracked grain boundaries as a function of aging time at 170°C.

practice (48 hr. at 170°C) allows alloy LC1 to obtain approximately 90% of its maximum strength without causing severe secondary cracking.

2.3.8 Effect of Thermomechanical Processing

The thermomechanical processing methods (TMP) described in Section 2.2.9 were used to recrystallize alloys LC1 and LCM1, in an effort to increase the grain boundary area per unit volume. Such treatments were originally developed for grain size control in AA 7475 alloys [24,25], where the object is to render the alloys superplastic.

We first tried the following treatments on the alloy LCM1:

TMP1: SHT 30 min./550°C
aging 8 hr./450°C
rolling 80% at 250°C
recrystallization 1 hr./550°C

TMP2: SHT 30 min./550°C
aging 8 hr./450°C
aging 8 hr./350°C
rolling 80% at 250°C
recrystallization 1 hr./550°C

Severe cracking occurred during rolling for both specimens. This is not surprising, since some cracks must have appeared in the SHT step, as indicated in section 2.3.3. At the time these treatments were used, the phenomenon of intergranular fracture during solution heat treatment had not yet been recognized.

Grain structure proved to be recrystallized in both specimens, with a more complete recrystallization after treatment TMP2. This is a consequence of the additional 8 hr./350°C aging step included in treatment TMP2. The additional aging step lowers the concentration of alloying elements in solid solution, thus reducing the boundary drag pressure from solute atoms during recrystallization. The added treatment also promotes a coarser precipitation of intermetallic phases,

which increases the number of sites for nucleation of new grains [25]. However, the extent of cracking during rolling was so great that these specimens were of little use for anything but microstructural observation.

After identifying the phenomenon of intergranular fracture during solution treatment of alloy LCM1 at 550°C, additional processing experiments were performed. Treatment TMP2 was used on both alloy LC1 with the 550°C SHT temperature, and on alloy LCM1 with a temperature of 530°C instead of 550°C (designated TMP3).

Recrystallization in this set of specimens was not uniform, as shown in Figure 12: the left side of tensile specimen LCM1.T3 is fully recrystallized (compare with Figure 1), whereas the other side is only partly recrystallized.

Tensile specimens were prepared from the processed materials, and the fracture surfaces were examined to see if recrystallization had produced a change in the extent of intergranular fracture. The incidence of intergranular fracture was lower across the entire fracture surface, compared to the non-TMP specimens. This indicates that the grain size affects intergranular fracture of these materials, which may be accounted for by one of the following explanations:

i. a finer grain size reduces the slip length , and consequently lowers the stress concentrated at grain boundaries due to either grain boundary precipitates [19] or slip bands.

ii. elements such as K, Na or Ca, known to segregating at grain boundaries and lowering their cohesion, are diluted by the increased grain boundary area per unit volume [4].

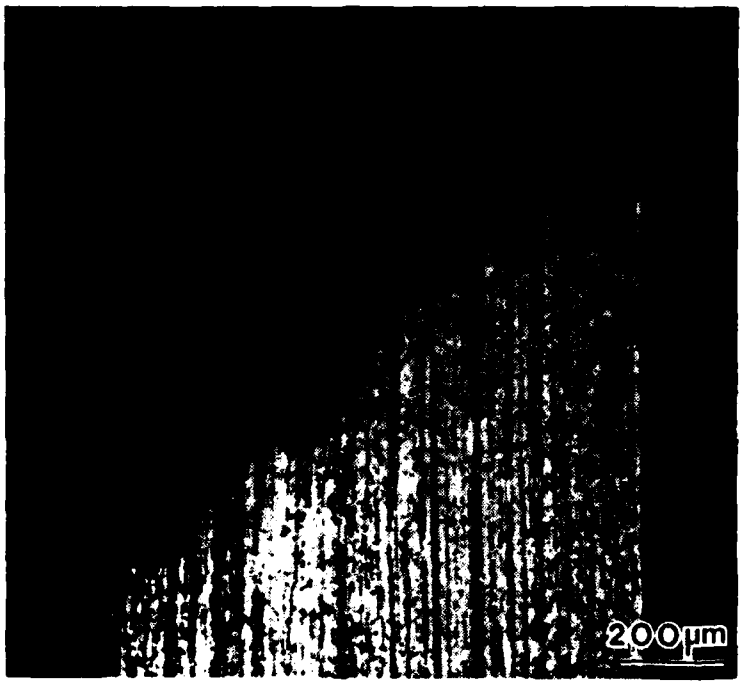

Fig. 12 Sectioned tensile specimen, thermomechanically processed then tested to failure. Alloy LCM1.TMP3. (TS plane)

Based on the experiments conducted in this investigation, it appears that TMP for recrystallization may be a useful method for reducing the incidence of intergranular fracture during tensile deformation. However, the present alloys, which contain more than 0.1 wt.% Zr, are extremely resistant to recrystallization. In the present study, we were unable to obtain a uniform microstructure through the thickness of the processed materials. Thus, this avenue could not be further pursued.

2.4. Discussion

2.4.1 Intergranular Fracture During Solution Treatment and Quench

This study has shown that intergranular fracture of an Al-Li-Cu-Mg alloy with the composition of alloy LCM1 can occur during solution treatment alloy LCM1 at 550°C without application of an external stress. Lower solution treatment temperatures did not produce intergranular fracture. In addition, intergranular fracture was only observed in conjunction with a grain boundary phase having the same crystal structure and lattice parameter as the aluminum matrix.

This evidence indicates that nonequilibrium eutectic melting occurs when alloy LCM1 is heated to a solution treatment temperature of 550°C at a heating rate of 2°C or faster. Figure 13 shows how nonequilibrium eutectic melting is consistent with the observations. A particle present at a boundary between grains I and III will normally be taken into solid solution if the heating rate is sufficiently modest to maintain equilibrium. At rapid heating rates, the particle is not taken into solid solution before the temperature exceeds the eutectic temperature, causing melting in the matrix adjacent to the interface between the particle and the matrix. If the solid-liquid interfacial energy is lower

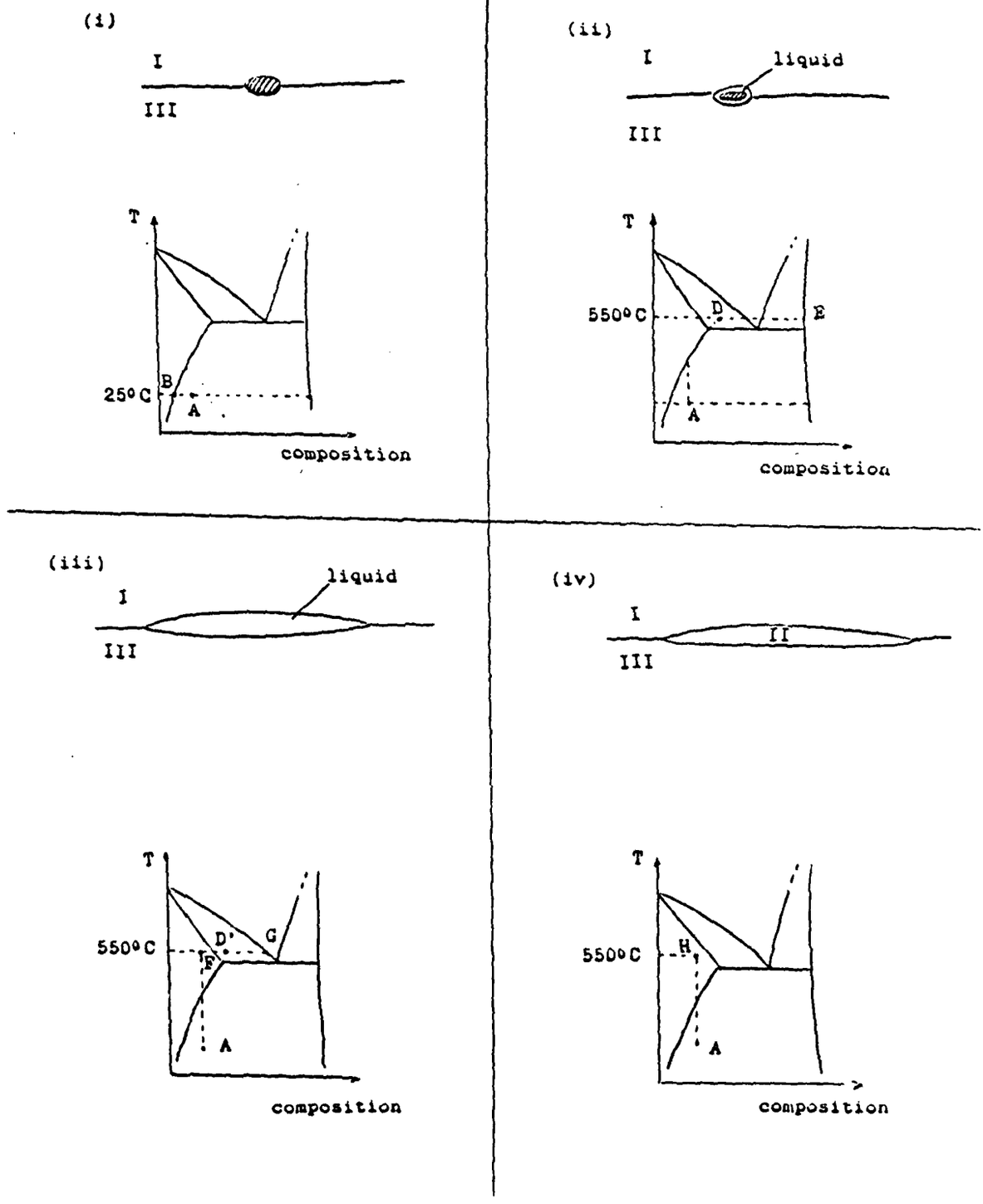

Fig. 13 Schematic diagrams showing relationship between nonequilibrium eutectic melting and the appearance of grain boundary phase in solution treated specimens.

than the grain boundary energy, the liquid will spread out as a thin layer along the boundary. Fracture may or may not occur at this point, depending on the local thermal stress state.

As solution treatment continues, the excess solute present in the liquid diffuses into the adjoining aluminum grains, causing the liquid to solidify in the form of a thin grain of aluminum interposed between the original grains I and III. Fracture may also occur upon solidification or during quenching. Our experiments have not been able to reveal at which point fracture occurs.

Although we could not observe the liquid phase at grain boundaries, the nonequilibrium melting explanation is consistent with all of the evidence that has been gathered in the present investigation. Nonequilibrium eutectic melting also occurs in other aluminum alloy where it is commonly termed "overheating". Overheating is usually encountered in commercial production of aluminum alloys during homogenization of cast ingots, although it can also occur during solution treatment if the heating rate is high.

The difference between the prior observations and those made in the present study is the morphology of the liquid phase. In previous investigations, the liquid has remained adjacent to the particles instead of spreading out as a thin film along grain boundaries. This difference in liquid phase morphology between alloy LCM1 and other alloys in which overheating has been observed must be due to a lower liquid-solid interface energy in the case of the Al-Li-Cu-Mg alloy. It seems likely that the lithium addition causes the difference in interfacial energy because the intergranular film morphology has not been reported in Al-Cu-Mg alloys. Of the alloying elements present is alloys LC1 and

LCM1, Li is known to decrease the liquid-vapor interfacial energy more strongly than either Cu or Mg [26]. However, solid liqiud interfacial energies have not been measured for Al-Li-base alloys, and consequently we are unable to independently confirm the relationship between the solid-liquid interfacial energy and the grain boundary energy implied by our observations.

An effort was made to establish which phase caused nonequilibrium eutectic melting in alloy LCM1 by locating a grain boundary particle in conjunction with the grain boundary phase in a TEM specimen solutionized for a short time (1 minute) at 550°C. Longer solution treatment times allow the intermetallic particles to dissolve completely, precluding their observation. One such occurrence was observed, as described previously. However, since the liquid phase could penetrate along the grain boundary over a length of more than 1 mm, it was not possible to conclude that the particular particle under observation was responsible for formation of the liquid phase. We were unable to identify the phase responsible for nonequilibrium eutectic melting in this study.

Shamray and Fridlyander reported equilibrium eutectic melting in Al-Li-Cu-Mg alloys. In alloys falling within the Al-Al_2CuMg-Al_2CuLi phase field, the eutectic temperature was reported to be 505°C. Other phase fields were reported to have higher eutectic melting temperatures. Unfortunately, we were unable to establish the composition of the particles responsible for formation of the liquid phase. This prevents detailed analysis of the results of the present investigation using the observations of Shamray and Fridlyander.

Webster has suggested that the low toughness of Al-Li-base alloys of various types is attributable to liquid phases formed by Na and K impurities at aging temperatures near 170°C. However, according to Webster, the Na and K responsible for formation of the liquid phases are in solid solution at the solution treatment temperature. Therefore, the intergranular phase observed in the present case in quenched specimens could not be the same phenomenon proposed by Webster. Moreover, the Na concentrations in the present alloys are very low compared to the levels contained in alloys examined by Webster.

2.4.2 Intergranular Fracture During Tensile Deformation.

Evidence described in the previous section shows that some intergranular cracks in alloy LCM1 are caused by nonequilibrium eutectic melting at a solution treatment temperature of 550°C. However, the eutectic melting phenomenon cannot be responsible for intergranular fracture during tensile deformation of alloy LCM1 when solution treatment temperatures of 530°C and below were employed. Moreover, eutectic melting cannot account for intergranular fracture of alloy LC1 during tensile deformation.

Thus, at least one additional mechanism of intergranular fracture must be operative in the alloys used in the present investigation. As discussed in the introduction, the explanations proposed for intergranular fracture of Al-Li-base alloys fall into four broad categories [1-14]: stress concentration due to planar slip, strain localization in PFZs, grain boundary particles, and segregation of Na and K impurities to grain boundaries. A fifth category, nonequilibrium eutectic melting during solution treatment, can be added to the list of possible causes based on results of the present investigation.

The Na and K concentration in alloys LC1 and LCM1 can be converted into a grain boundary concentration by assuming that all of the Na and K is segregated to the grain boundaries. This calculation yields upper bounds for the grain boundary concentrations of Na and K, denoted $(GBC)_{Na}$ and $(GBC)_{K}$. Values for these parameters are included in Table 2.3, for the present investigation and for two previous investigations. It can be seen that the upper bound grain boundary concentrations of Na and K in the present alloys are quite low compared to the concentrations in alloys studied by Vasudevan and coworkers and by Wert and Lumsden. In particular, $(GBC)_{Na}$ in alloys LC1 and LCM1 is substantially lower than the value of $(GBC)_{Na}$ found by Vasudevan and coworkers to produce exclusively intergranular fracture in as-quenched Al-Li-Mn-(Na) alloys. Thus, it appears unlikely that grain boundary fracture is caused by these impurity elements in the present case.

Table 2.3
Grain Structure Characteristics

Alloy	Grain Intercept Length*, μm	S_V m^{-1}	$(GBC)_{Na}$ mol/m²	$(GBC)_{K}$ mol/m²
LC1	18	5.6×10^{4}	2.8×10^{-5}	5.9×10^{-6}
LCM1	40	2.5×10^{4}	2.7×10^{-5}	1.3×10^{-5}
[5]	--	2.5×10^{4}	1.4×10^{-5}	2.9×10^{-4}
[2]	--	7.6×10^{3}	5.2×10^{-5}	5.2×10^{-5}
[2]	--	7.6×10^{3}	7.0×10^{-4}	5.2×10^{-5}
[2]	--	7.6×10^{3}	7.4×10^{-3}	5.2×10^{-5}

Concerning the remaining proposed explanations, it is impossible to distinguish between these, based solely on the results of the present investigation. The fraction of cracked grain boundaries increases

substantially with aging time at 170°C for alloy LC1, and slightly for alloy LCM1. Any of the remaining proposed explanations are consistent with these observations.

2.5 Conclusions

This investigation has examined intergranular fracture during heat treatment and deformation of an Al-Li-Cu-Mg alloy. When solution treatment is carried out in a salt bath at a temperature of 550°C, nonequilibrium eutectic melting of a soluble phase occurs in this alloy. The liquid spreads along grain boundaries as a thin film, which solidifies by diffusion of solute into the adjoining grains. Upon quenching, intergranular cracks are found in conjunction with grain boundaries where a liquid film had formed during solution treatment. At solution treatment temperatures of 530°C and below, nonequilibrium eutectic melting did not occur and no intergranular cracks were found in as-quenched specimens. The eutectic melting is associated with a soluble phase. No evidence of nonequilibrium eutectic melting was found in a companion Al- Li-Cu alloy.

For the Al-Li-Cu-Mg alloy, intergranular fracture occurred during tensile testing of as-quenched and quenched-and-aged specimens, irrespective of whether nonequilibrium eutectic melting had taken place during solution treatment. For the Al-Li-Cu alloy, intergranular fracture occurred during tensile testing of quenched-and-aged specimens, but not of as-quenched specimens. The cause of intergranular fracture during deformation of the present alloys is unlikely to be segregation of Na and K impurities to grain boundaries. Several additional explanations for intergranular fracture have previously been proposed, but the available evidence in the present

case does not strongly support or exclude any of the remaining explanations

2.6 References

1. E.A. Starke Jr. and T.H. Sanders Jr., Journal of Metals, August, 1981, pp. 24-32.

2. A.K. Vasudevan, A.C. Miller and M.M. Kersker, in "Aluminum Lithium Alloys II", T.H. Sanders Jr. and E.A. Starke Jr. (eds), The Metallurgical Society of AIME, Warrendale, PA, 1984, pp. 181-199.

3. S.J. Harris, B. Noble and K. Dinsdale, in "Aluminum Lithium Alloys II", T.H. Sanders Jr. and E.A. Starke Jr. (eds), The Metallurgical Society of AIME, Warrendale, PA, 1984, pp. 219-233.

4. P.E. Bretz, L.N. Mueller and A.K. Vasudevan, in "Aluminum Lithium Alloys II", T.H. Sanders Jr. and E.A. Starke Jr. (eds), The Metallurgical Society of AIME, Warrendale, PA, 1984, pp. 543-559.

5. J.A. Wert and J.B. Lumsden, Scripta Met. 19 (1985) 205.

6. P.J. Doorbar, J.B. Borradaile and D. Driver, in "Aluminum-Lithium Alloys III", C. Baker, P.J. Gregson, S.J. Harris and C.J. Peel (eds), The Institute of Metals, London, 1986, pp. 496-508.

7. P.J.E. Bischler and J.W. Martin, in "Aluminum Lithium Alloys III", C. Baker, P.J. Gregson, S.J. Harris and C.J. Peel (eds), The Institute of Metals, London, 1986, pp. 539-546.

8. W.S. Miller, M.P. Thomas, D.J. Lloyd and D. Creber, in "Aluminum-Lithium Alloys III", C. Baker, P.J. Gregson, S.J. Harris and C.J. Peel (eds), The Institute of Metals, London, 1986, pp. 584-594.

9. S. Suresh and A.K. Vasudevan, in "Aluminum Lithium Alloys III", C. Baker, P.J. Gregson, S.J. Harris and C.J. Peel (eds), The Institute of Metals, London, 1986, pp. 795-801.

10. D. Webster, in "Aluminum Lithium Alloys III", C. Baker, P.J. Gregson, S.J. Harris and C.J. Peel (eds), The Institute of Metals, London, 1986, pp. 602-609.

11. A.K. Vasudevan, E.A. Ludwiczak, S.F. Baumann, E.R. Howell, R.D. Doherty, M.M. Kersker, Mat. Sci. Technology, 2 (1986) 1205.

12. R.C. Dorward, J. Mat. Sci. Letters, 5 (1986) 1181.

13. W.S. Miller, M.P. Thomas, D.J. Lloyd and D. Creber, Mat. Sci. Technoogy, 2 (1986) 1210.

14. N.J. Owen, D.J. Fieldand, E.P. Butler, Mat. Sci. Technology, 2 (1986) 1217.

15. M.J. Bull and D.J. Lloyd, in "Aluminum-Lithium Alloys III", C. Baker, P.J. Gregson, S.J. Harris and C.J. Peel (eds), The Institute of Metals, London, 1986, pp. 402-410.

16. R.F. Ashton, D.S. Thompson, E.A. Starke, Jr. and F.S. Lin, in "Aluminum Lithium Alloys III", C. Baker, P.J. Gregson, S.J. Harris and C.J. Peel (eds), The Institute of Metals, London, 1986, p. 66-77.

17. "Aluminum Lithium Alloys II", T.H. Sanders Jr. and E.A. Starke Jr. (eds), TMS-AIME, Warrendale, PA, 1983.

18 "Aluminum Lithium Alloys III", C. Baker, P.J. Gregson, S.J. Harris and C.J. Peel (eds), The Institute of Metals, London, 1986.

19 M.E. O'Dowd, "The Influence of Precipate Type on Elastic Properties of Al-Cu-Li Alloys", Masters Thesis, UVa, Jan. 1987.

20 W.A. Cassada, G.J. Shiflet and E.A. Starke, Jr., Scripta Met., 20 pp. 751-756, 1986.

21 W.A. Cassada, G.J. Shiflet and E.A. Starke, Jr., Scripta Met., 20 pp. 751-756, 1986.

22 P. Sainfort, B. Dubost and A. Dubus, C.R. Acad. Sc. Paris, Serie II, 301 (1985) 689.

23 P. Sainfort and B. Dubost, 1986 "The T_2 Compound: A Stable Quasi-Crystal in the System Al-Li-Cu-(Mg)", preprint.

24 J.A. Wert, N.E. Paton, C.H. Hamilton and M.W. Mahoney, Met. Trans. 12A (1984) 1267.

25 J.A. Wert, "Thermomechanical Processing of Heat Treatable Aluminum Alloys for Grain Size Control", E.H. Chia and H.J. McQueen (eds.), The Metallurgical Society of AIME, Warrendale, 1982, pp. 67-94.

26 J.E. Hatch, "Aluminum: Properties and Physical Metallurgy", American Society for Metals, Metals Park, 1984, p. 209.

Appendix

Tensile Properties of Alloys LC1 and LCM1 After Heat Treatment

SPECIMEN	SHT TIME (min)	SHT TEMP (C)	AGING TIME (hr)	AGING TEMP (C)	YIELD STRESS (MPa)	TENSILE STRENGTH (MPa)	ELONG. (%)
LC1.4	30	550	0	-	156.1	317.9	16.2
LC1.1	30	550	24	190	404.0	464.1	4.0
LC1.2	30	550	48	190	400.4	455.9	4.4
LC1.3	30	550	96	190	386.0	436.3	5.2
LCM1.4	30	550	0	-	306.4	439.9	10.7
LCM1.1	30	550	24	190	490.4	558.3	4.0
LCM1.2	30	550	48	190	478.8	541.6	6.0
LCM1.3	30	550	96	190	465.2	525.5	5.2
LC1.5	30	550	48	170	361.6	453.2	3.6
LC1.6	30	550	192	170	425.9	486.4	3.6
LC1.7	30	550	600	170	360.6	436.1	4.8
LCM1.5	30	550	48	170	424.7	518.9	5.6
LCM1.6	30	550	192	170	492.1	572.5	3.6
LCM1.7	30	550	600	170	462.3	518.5	0.8
LC1.9	30	530	0	-	151.8	308.5	15.8
LC1.10	30	530	192	170	447.0	510.2	7.0
LC1.11	30	530	16	190	363.4	461.0	4.3
LCM1.9	30	530	0	-	297.8	436.0	11.7
LCM1.10	30	530	192	170	467.0	563.8	4.2
LCM1.11	30	530	16	190	420.2	523.4	5.9
LCM1.12	30	500	0	-	274.6	475.9	8.4
LCM1.14	500 to 530/60 min		0	-	255.1	459.2	9.2

Tensile Properties of Alloys LC1 and LCM1 After TMP and Heat Treatment

SPECIMEN	SHT/RECR TIME (min)	SHT/RECR TEMP (C)	AGING TIME (hr)	AGING TEMP (C)	YIELD STRESS (MPa)	TENSILE STRENGTH (MPa)	ELONG. (%)
LC1.T3	60	550	0	190	139.8	274.5	25.4
LC1.T4	60	550	24	190	402.2	449.8	3.0
LCM1.T2	60	550	24	190	424.9	516.5	4.2
LCM1.T3	60	530	0	190	297.7	444.0	17.0
LCM1.T4	60	530	24	190	406.2	509.0	8.1

DISTRIBUTION LIST

Copy No.	
1 - 16	Air Force Office of Scientific Research/NE Building 410 Bolling Air Force Base Washington, D.C. 20332 Attention: Alan H. Rosenstein
17 - 18	E. A. Starke, Jr.
19 - 20	J. A. Wert, MS
21	T. H. Courtney, MS
22 - 23	E. H. Pancake Clark Hall
24	SEAS Publications Files

UNIVERSITY OF VIRGINIA
School of Engineering and Applied Science

The University of Virginia's School of Engineering and Applied Science has an undergraduate enrollment of approximately 1,500 students with a graduate enrollment of approximately 560. There are 150 faculty members, a majority of whom conduct research in addition to teaching.

Research is a vital part of the educational program and interests parallel academic specialties. These range from the classical engineering disciplines of Chemical, Civil, Electrical, and Mechanical and Aerospace to newer, more specialized fields of Biomedical Engineering, Systems Engineering, Materials Science, Nuclear Engineering and Engineering Physics, Applied Mathematics and Computer Science. Within these disciplines there are well equipped laboratories for conducting highly specialized research. All departments offer the doctorate. Biomedical and Materials Science grant only graduate degrees. In addition, courses in the humanities are offered within the School.

The University of Virginia (which includes approximately 2,000 faculty and a total of full-time student enrollment of about 16,400) also offers professional degrees under the schools of Architecture, Law, Medicine, Nursing, Commerce, Business Administration, and Education. In addition, the College of Arts and Sciences houses departments of Mathematics, Physics, Chemistry and others relevant to the engineering research program. The School of Engineering and Applied Science is an integral part of this University community which provides opportunities for interdisciplinary work in pursuit of the basic goals of education, research, and public service.

END

7-87

DTIC